Aus dem Department für Diagnostische Labormedizin der Universität Tübingen

Sektion Zelluläre und Molekulare Mikrobiologie

Biogenesis of the core components SpaP, SpaQ and SpaR of the Salmonella type III secretion system

Inaugural-Dissertation
zur Erlangung des Doktorgrades
der Medizin

der Medizinischen Fakultät
der Eberhard Karls Universität
zu Tübingen

vorgelegt von
Forberger, Mirjam

2022

Dekan: Professor Dr. B. Pichler

1. Berichterstatter: Professor S. Wagner, PhD
2. Berichterstatter: Privatdozentin Dr. M. Schütz

Tag der Disputation: 23.04.2021

Table of contents

Table of contents I
Abbreviations III
List of figures and tables IV
1 Introduction 1
1.1 Pathogenicity of *S.* Typhimurium 1
1.2 Components of the Type III Secretion System 3
1.3 Assembly of the Type III Secretion System 5
1.4 Protein structure and interactions of the export apparatus 7
1.5 Genetic conservation and regulation of the export apparatus 9
1.6 mRNA structure 12
1.7 Objectives 13
2 Material and Methods 14
2.1 Antibodies, buffers, media 14
2.2 Culture conditions 16
2.2.1 Bacterial growth and storage 16
2.2.2 Protein overexpression induced with L-rhamnose 16
2.3 Cloning procedures 17
2.3.1 Gibson Assembly 17
2.3.2 QuikChange site-directed mutagenesis 18
2.3.3 Megaprimer mediated mutagenesis 19
2.4 BN PAGE and Sodium dodecyl sulfate polyacrylamide gel electrophoresis (SDS PAGE) 19
2.4.1 Crude Membranes 20
2.4.2 BN PAGE 21
2.4.3 SDS-PAGE of whole bacteria 21
2.4.4 Western Blotting 22
2.5 SipA luciferase-based secretion assay 22
2.6 Tables of materials 23
3 Results 36
3.1 Selection of the constructs to be examined 36

3.2 Creating the best starting conditions: Optimization of rhamnose induction 40
3.3 Changes in the gene sequence affect protein expression, complex formation and secretion activity 41
3.4 Further investigation of SpaQ remnant 47
3.5 Influence of *spaQ* 49
3.6 Technical limitations 56
4 Discussion 51
4.1 *spaQ* has a regulatory function in the assembly of the export apparatus 52
4.2 The wrong stoichiometry leads to self-assembly 53
4.3 Overexpression of *spaR* 55
4.4 Conclusion 56
5 Outlook 58
6 Summary 60
7 Deutsche Zusammenfassung 61
8 Literature 62
9 Appendix 67
10 Erklärung zum Eigenanteil 68
11 Danksagung 70

Abbreviations

BN	Blue Native
bp	base pairs
Bpa	*para*-benzoyl-L-phenylalanine
ddH_2O	double deionized water
DMSO	dimethyl sulfoxide
dNTP	deoxynucleotide triphosphate
E. coli	*Escherichia coli*
EDTA	ethylenediaminetetraacetic acid
et al.	and others
kDa / MDa	kilodalton / megadalton
LB	Luria broth
LMNG	lauryl maltose neopentyl glycol
OD_{600}	optical density at a wavelength of 600 nm
ODU	optical density units (per milliliter)
PAGE	polyacrylamide gel electrophoresis
PBS	phosphate buffered saline
PCR	polymerase chain reaction
QC	QuikChange site-directed mutagenesis
rpm	revolutions per minute
SD	Shine-Dalgarno
SDS	sodium dodecyl sulfate
SOB	super optimal broth
SOC	super optimal broth with catabolite repression
SPI-1	*Salmonella* pathogenicity island 1
SPI-2	*Salmonella* pathogenicity island 2
S. Typhimurium	*Salmonella* Typhimurium
T3SS	type III secretion system
Taq	*Thermus aquaticus*
TBS	Tris-buffered saline
TBS-T	Tris-buffered saline supplemented with Tween 20
TMD	transmembrane domain
Tris	tris (hydroxymethyl) aminomethane

For amino acids, the common IUPAC 1-letter code has been used. Nucleotides are shown in lower case.

List of figures and tables

Table 1: List of antibodies used 14
Table 2: Contents of buffers and media 14
Table 3: Concentrations of the antibiotics used 16
Table 4: QuikChange PCR setup 18
Table 5: Megaprimer PCR setup 19
Table 6: List of bacteria used 23
Table 7: List of primers used 23
Table 8: List of plasmids used 25
Table 9: Relative secretion activity compared to the wild type. 67

Figure 1: Enteroinvasion of *S*. Typhimurium into the intestinal epithelium 2
Figure 2: Schematic overview of the individual components of the fully assembled T3SS. 4
Figure 3: Assembly of the export apparatus and location inside the fully assembled T3SS. 6
Figure 4: Complex formation and structural homology of $SpaP_5Q_4R_1$ complex. 7
Figure 5: Charge and hydrophobicity on the surface of the PQR complex. 8
Figure 6: The membrane protein character with TMDs is still visible in the SpaPQR complex. 9
Figure 7: Comparison of the genetic organisation of *spaPQRS* and their homologs in flagella (*E. coli*) and *Yersinia*. 11
Figure 8: Predicted mRNA folding of *spaR* and *spaQ* and possible topological difficulties. 13
Figure 9: Difference of the SD sequences and the *spaP-spaR* transition of $P^{\wedge L}RQS$ and $P^{\wedge S}RQS$ 39
Figure 10: Plasmid pTACO10 and different constructs with alternated gene order (overview). 37
Figure 11: Optimization of rhamnose induction. 41
Figure 12: Comparison of the complex assembly and NanoLuc-luciferase signal as a measure of the secretion activity in constructs with different gene order. 42
Figure 13: Comparison of the complex assembly and NanoLuc-luciferase signal as a measure of the secretion activity in constructs with different *spaP-spaR* transition. 43
Figure 14: Effect of the peptide SpaQ remnant on complex assembly 48
Figure 15: Direct comparison of constructs with and without *spaQ* or *spaS* of different FLAG-tags. 50
Figure 16: Possible defective assembly complexes of the export apparatus 55
Figure 17: NanoLuc-luciferase signal as a measure of the secretion activity from different constructs in percentage of the wild type *spaPQRS*$^+$. 67

Introduction

Every year, an estimated 93.8 million people worldwide suffer from non-typhoidal salmonellosis (Majowicz et al. 2010). In humans, *Salmonella enterica* serovar Typhimurium (hereafter referred to as *S.* Typhimurium) is one of the four most common pathogens causing diarrhea (World Health Organization 2020). In the majority of immunocompetent people, an infection leads to self-limiting diarrhea. However, especially in children, the elderly and also in developing countries, a more severe and complicated course is more likely (World Health Organization 2020). In crisis areas and after environmental disasters a higher rate of infection can be observed, which can also be explained by the transmission route.

1.1 Pathogenicity of *S.* Typhimurium

Salmonella can be transmitted from person to person fecal-orally via smear infection, contaminated water or food. Eggs, meat and cheese are the most common sources. In Germany, salmonellosis is the sixth most common notifiable infectious disease with over 13 500 reported cases per year (Robert-Koch Institut 2019). However, the proportion of reported cases of illness is estimated to be only 10 to 20% of actual cases (Bundesinstitut für Risikobewertung 2020).

Various pathogenicity factors can make microorganisms dangerous for the human organism. In addition to bacteria that produce exotoxins such as *Vibrio cholerae*, many others manifest their pathogenicity through adhesion, invasion and subsequent tissue damage (Eitinger 2017). This is also the case for *Salmonella*.

S. Typhimurium can be absorbed from the intestine (Figure 1 a) via microfold (M)-cells located in the Peyer patches (Bradley 1994). Like *Yersinia* spp. and *Shigella* spp., *S*. Typhimurium also has the specialty of injecting effector proteins directly into the target cells using a needle-like complex - the so-called type III secretion system (T3SS) or injectisome. There are two different T3SS encoded on the so-

called *Salmonella* pathogenicity islands 1 and 2 (SPI-1 and SPI-2). The effector proteins of the SPI-1 T3SS enable *S*. Typhimurium to invade intestinal cells by causing rearrangement of the actin cytoskeleton and membrane ruffling in the membrane (Figure 1 b) of the primary non-phagocytizing target cell (Hansen-Wester and Hensel 2001). As a result, the bacterium is enclosed and finally taken up into a phagosomal compartment, the *Salmonella* containing vacuole (SCV) (Zhou 1999).

Once inside the cell, *S*. Typhimurium has the ability to produce various effectors and translocate them into the cytoplasm using the SPI-2 T3SS. These effectors contribute to preserve the integrity of the SCV. (Figueira and Holden 2012, Eitinger 2017).

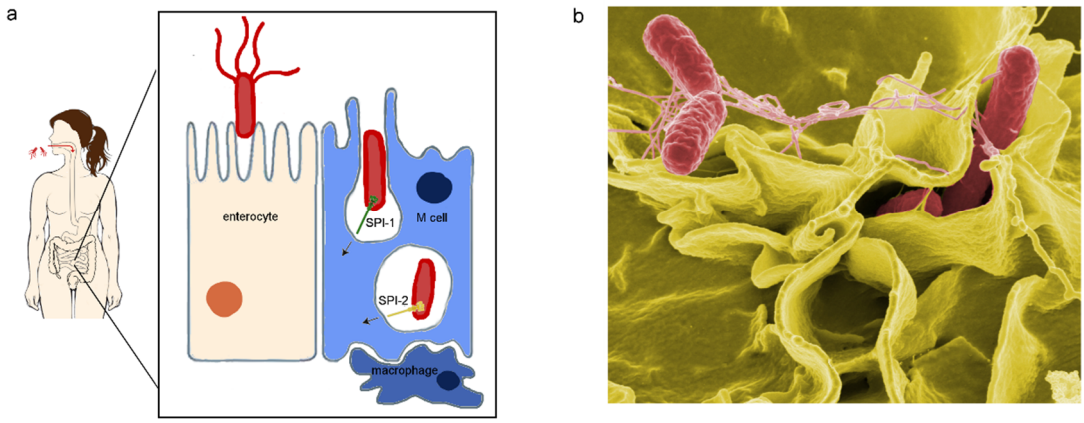

Figure 1: Enteroinvasion of *S.* Typhimurium into the intestinal epithelium.
(a) *S*. Typhimurium is taken up orally via contaminated water or food and enters the intestinal epithelium preferably via M-cells using the Type III Secretion System (T3SS). On the chromosome of *Salmonella* are two different *Salmonella* pathogenicity islands (SPI), each coding for a different T3SS. T3SS encoded on SPI-1 (shown here in green) enables uptake into the enterocytes, T3SS encoded on SPI-2 (shown in yellow) inhibits antimicrobial activities and helps to preserve the intactness of the Salmonella-containing vacuole (SCV). (Modified after Haraga et al. 2008:55)
(b) *S*. Typhimurium (red) invading cultured human cells. Colored electron microscope scan from the National Institute of Allergy and Infectious Diseases, Source: Wikimedia commons.

1.2 Components of the Type III Secretion System

The fully assembled T3SS consists of a base, cytoplasmic components, export apparatus and needle with translocon (Figure 2).

The base is composed of an outer and an inner ring. The outer ring is an outer membrane secretin complex, which consists of 12-15 units of InvG (Wagner et al. 2018). It protrudes into the periplasm and surrounds the proximal part of the needle. The inner ring is divided into two concentric rings, which are formed by 24 units of PrgH on the outside and 24 units of PrgK on the inside. PrgH functions as a connecting element both to the outer membrane ring InvG and to OrgA of the cytosolic components (Wagner et al. 2018).

OrgA, OrgB and SpaO probably play a role in the recruitment of export proteins in the respective secretion phase and therefore form the so-called sorting platform (Lara-Tejero et al. 2011). In the center of the cytosolic components is located the hexameric proton motive force driven ATPase InvC. This is connected to the export apparatus by InvI (Wagner et al. 2018).

The export apparatus consisting of five proteins is centrally located and spans the inner membrane. The core of this apparatus is formed by SpaR, SpaQ and SpaP, which together form a helical complex with a central passage. At the proximal end is a circular complex of 9 InvA subunits, which is involved in the unfolding and removal of the chaperones of the substrates. InvA is followed by the switch protein SpaS, which attaches itself in an extension to the helically twisted spaPQR complex in the lower region and forms a loop around the export gate (Kuhlen et al. 2020). As its counterparts in the injectisome of *Yersinia* and the flagellar T3SS of *E.coli*, *Salmonella* SpaS undergoes autocleavage at the conserved amino acid sequence NPTH (Lavander et al. 2002). The autocleavage serves to increase the flexibility of SpaS and confers to the system the ability to secrete intermediate and late substrates (Monjarás Feria et al. 2015).

In the extension of the export apparatus 6 PrgJ subunits form a connection with the proximal part of the needle (Marlovits et al. 2006). The needle itself is made

up by more than 100 copies of the helically assembling PrgI protein, which form a pore through which effector proteins can be transported in an unfolded state. The tip of the needle is formed by a complex of several hydrophilic SipD proteins, which serve as a platform for two further translocators, SipB and SipC (Mueller et al. 2008). These proteins have transmembrane domains (TMDs) that integrate into the host cell, thus enabling cell penetration.

#	Uni	SPI-1
1	SctC	InvG
2	SctF	PrgI
3	SctI	PrgJ
4	SctJ	PrgK
5	SctD	PrgH
6	SctK	OrgA
7	SctQ	SpaO
8	SctL	OrgB
9	SctN	InvC
10	SctO	InvI
11	SctR	SpaP
12	SctS	SpaQ
13	SctT	SpaR
14	SctU	SpaS
15	SctV	InvA
16	SctE	SipB
17	SctB	SipC
18	SctA	SipD
19	SctP	InvJ
20	SctW	InvE

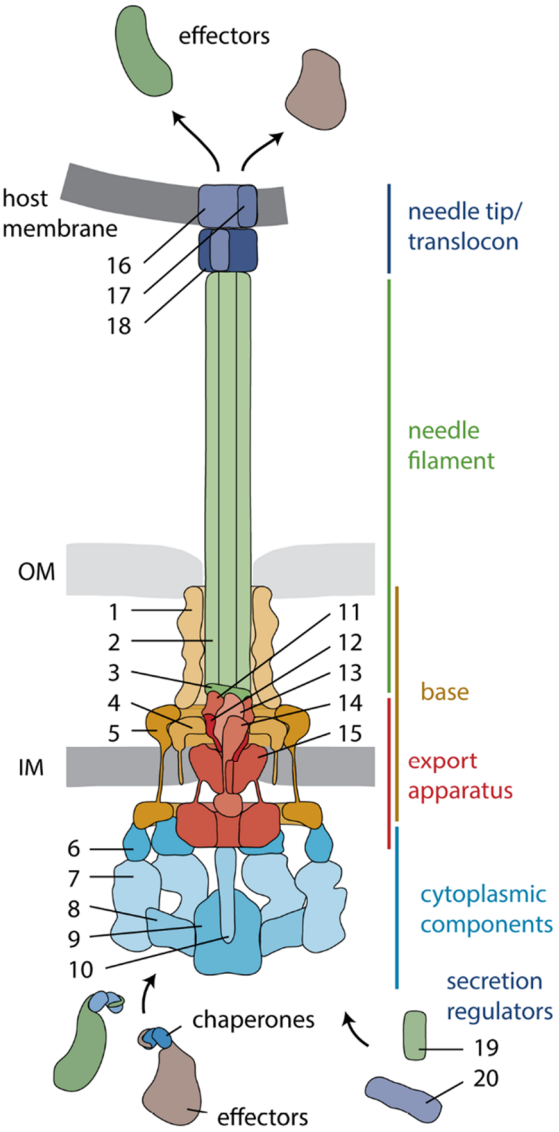

Figure 2: Schematic overview of the individual components of the fully assembled T3SS. Description of the individual components in unified nomenclature and SPI-1 of *S*. Typhimurium**.** OM: outer membrane, IM: inner membrane. (Wagner *et al*. 2018)

With such a complex machine, which spans three membranes when fully assembled, the question inevitably arises as to how the assembly can accurately work.

1.3 Assembly of the Type III Secretion System

The total T3SS complex is about 6 MDa in size and consists of 20 different proteins with copy numbers up to 100 (Zilkenat et al. 2016). Its assembly is therefore associated with high energy and resource consumption for the bacterium and is strictly regulated (Diepold and Wagner 2014).

The assembly starts with the export apparatus (Figure 3 a), which is examined in more detail in this study. The initial complex is formed by 5 helically assembling SpaP subunits, stabilized by 1 SpaR subunit (Dietsche et al. 2016). Subsequently, 4 SpaQ and 1 SpaS subunit assemble, followed by 9 InvA subunits (Abrusci et al. 2013, Kuhlen et al. 2018). Only the correct assembly of the export apparatus allows faultless assembly of a fully functional T3SS (Wagner et al. 2010).

Two different scenarios have been proposed. One is the outside-in assembly model and the other the inside-out assembly model. In both cases the export apparatus assembles first. In the outside-in model (Figure 3 b), PrgK is connected to the export apparatus and, independently of this, a complex of InvG is formed after hydrolysis of the cell wall peptidoglycan (PG) polymers by PG-lytic enzymes. With the help of pilotins, which are lipoproteins that guide other proteins to the outer membrane (Hardie et al. 1996), InvG assembles in a pre-pore and recruits PrgH. The outer ring of the inner membrane ring is only closed once the export apparatus and PrgK have been incorporated.

The inside-out model (Figure 3 c) describes the inner membrane ring forming around the export apparatus, followed by the cytoplasmic components. The still incomplete T3SS secretes early substrates into the periplasmic compartment, where they activate local PG-cleaving enzymes to create a pore for further assembly (Burkinshaw et al. 2015).

Common to both models is that the export apparatus pre-pore is formed on top of the inner membrane ring, which is then stabilized by proteins building the outer

membrane ring and completed by the gradual build-up of the needle (Figure 3 c). The correct needle length is ensured by the regulator protein InvJ.

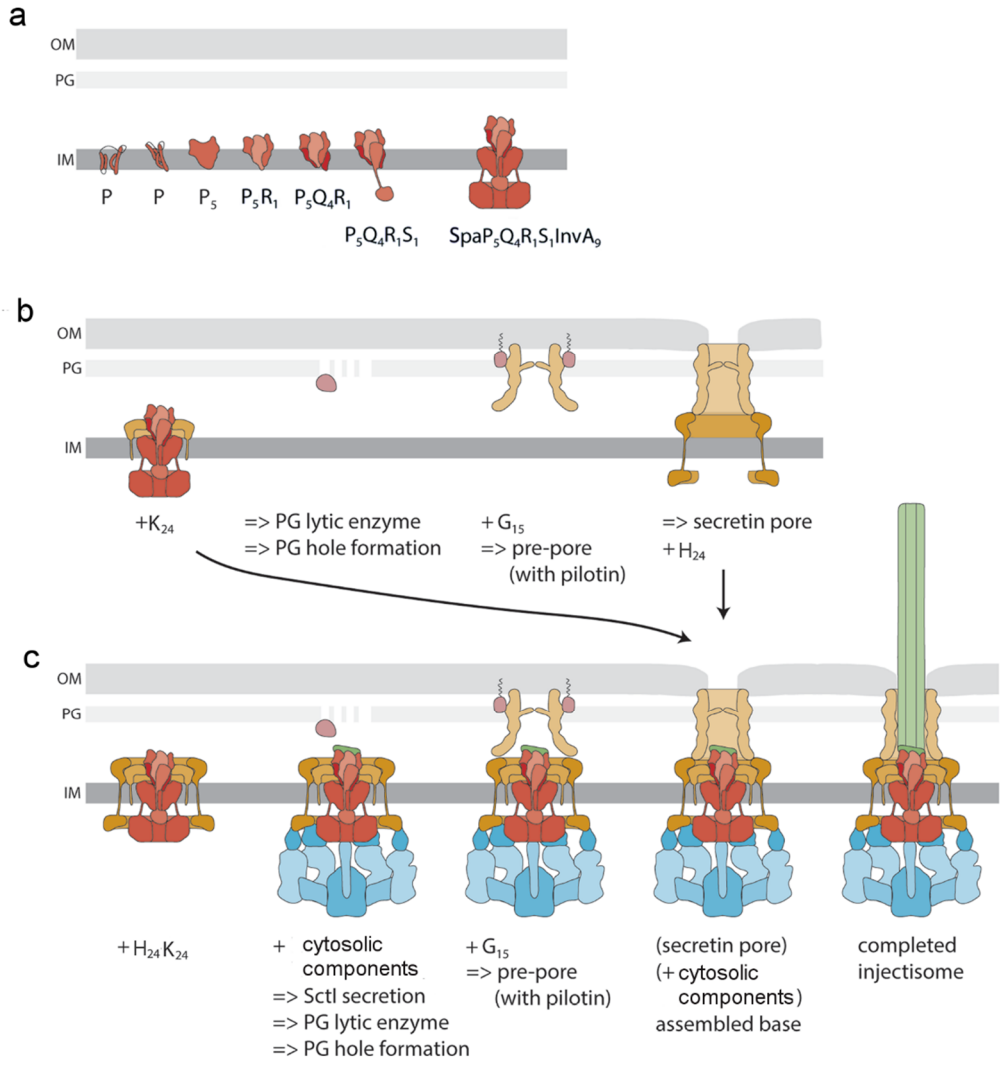

Figure 3: Assembly of the export apparatus and location inside the fully assembled T3SS. (a) Assembly of the export apparatus. P: SpaP. Schematic view of four TMDs and predicted folding. Starting with a self-assembled complex of 5 SpaP, followed by 1 SpaR and 4 SpaQ. Subsequent assembly of 1 SpaS and 9 InvA.
(b) Outside-in assembly model. PrgK assembles to the export apparatus. Independently, InvG assembles in a pre-pore and recruits PrgH. The outer ring of the inner membrane ring is only closed once the export apparatus and PrgK have been incorporated.
(c) Inside-out assembly model. Shell-wise assembly of the inner membrane ring of the base and the cytoplasmic components. The first phase of secretion allows the transport of peptidoglycan lytic enzymes and assembly of a pre-pore. OM: outer membrane, PG: peptidoglycan, IM: inner membrane (Wagner *et al.* 2018)

As soon as the needle makes contact with the host cell, the T3SS secretes the components for the needle tip and translocators. The translocators form a pore in the host cell membrane, which ultimately enables the transport of effectors from the bacterium directly into the cytoplasm of the host cell (Wagner et al.

2018). In absence of a host cell, T3SS-dependent effectors are secreted into the bacterial supernatant. In order to quantify this secretion, a reporter such as nanoluciferase (NanoLuc) can be used (Westerhausen et al. 2019).

1.4 Protein structure and interactions of the export apparatus

Bioinformatic models predict α-helical and hydrophobic components in SpaP, SpaQ, SpaR and SpaS (Goessweiner-Mohr et al. 2019). The whole complex of the export apparatus has a conical shape (Figure 4 a-c) and lies slightly tilted inside the membrane (Goessweiner-Mohr et al. 2019). Although the membrane proteins are highly hydrophobic, the assembly of the export apparatus apparently leads to a progressive twisting (Figure 4 d) of the complex out of the membrane (Kuhlen et al. 2018). The architecture is such that four subunits of SpaQ and SpaP are stacked on top of each other in a shape very similar to that of SpaR while the fifth SpaP subunit (P5, see Figure 4 a) remains without a counterpart.

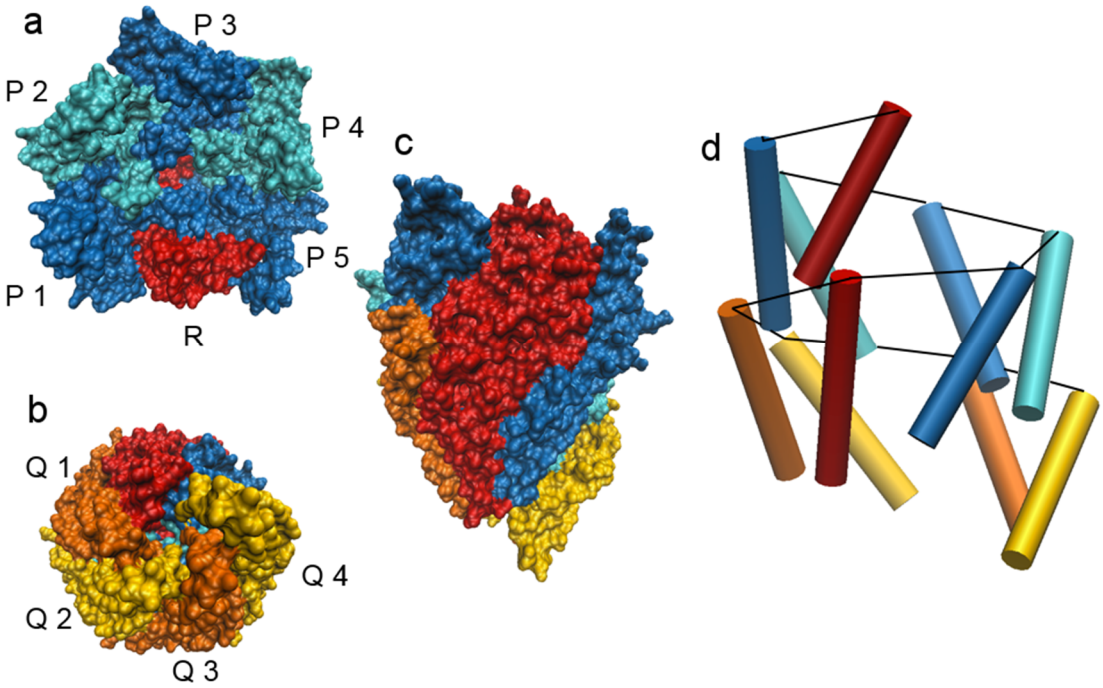

Figure 4: Complex formation and structural homology of the $SpaP_5Q_4R_1$ complex.
(a) Top view on the assembled $SpaP_5Q_4R_1$ complex. SpaP in blue, SpaR in red.
(b) Bottom view of (a). SpaQ in yellow and orange, SpaR in red.
(c) Side view of (a).
(d) Schematic view of helical winding. The structural similarity of SpaR as a fusion of SpaP and SpaQ is illustrated here. Colours as in (a)-(c). (Samuel Wagner, personal communication 2020)

The surface of the PQR complex has a charged upper part that partially protrudes from the membrane (Figure 5 a and c), and a hydrophobic, lower half with a hydrophilic part of SpaQ at the lowest peak (Figure 5 b and d). Whereas the hydrophobic surface components are largely contributed by SpaQ, the hydrophobic loops of SpaP and SpaR are partially located inside the complex. The inner surface that forms the export channel has been shown to be positively charged (Kuhlen et al. 2018).

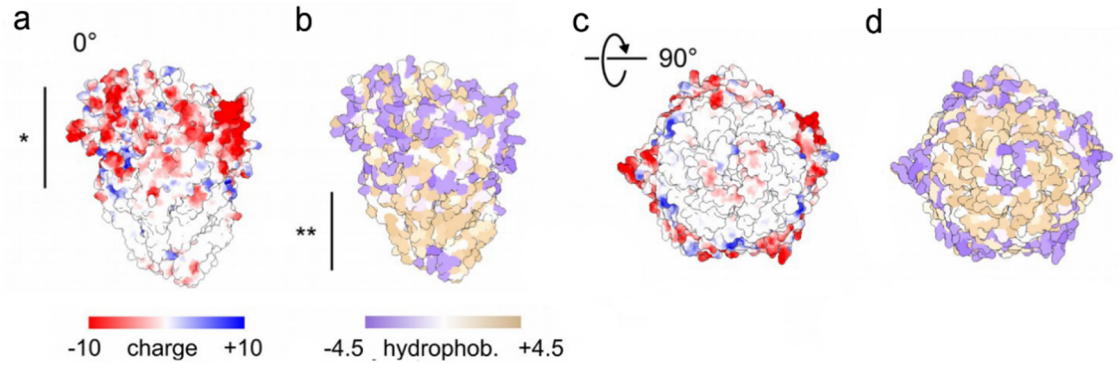

Figure 5: Charge and hydrophobicity on the surface of the PQR complex.
(a) Side view of the PQR complex. * charged belt, colors indicated below. Electrostatic potential was calculated on the basis of Coulomb's law.
(b) Side view of the PQR complex. ** hydrophobic belt. Scale according to Kyte and Doolittle (1982: 110).
(c) Bottom view of (a).
(d) Bottom view of (b). (Source: Goessweiner-Mohr et al. 2019:29)

Conserved charged amino acids of SpaP, SpaQ and SpaR are essential for intra- and intermolecular salt bridges (Kuhlen et al. 2018). SpaQ was found to be less stable in complexes of the virulence-associated T3SS than the homologue FliQ in the flagellar T3SS (Kuhlen et al. 2018). SpaS forms two helical hairpins, of which crosslinks to the outside of $SpaP_4$, $SpaP_5$ and SpaR have been detected. A loop encircles the export gate and contacts all 4 SpaQ subunits (Kuhlen et al. 2020).

SpaP, SpaQ and SpaR have a different number of α-helical TMDs (Figure 6 a). These hydrophobic regions suggest that co-translationally, they are first inserted into the membrane via the Sec-translocon system before they fold (Figure 6 b) and assemble in the complex (White and von Heijne 2004). After insertion into the membrane, the proteins must therefore undergo a structural rearrangement and wind themselves out of the membrane (Goessweiner-Mohr et al. 2019). SpaR represents a structural fusion of SpaP and SpaQ. Their basic structure is

made of transmembrane hairpins, which are after folding entangled in the assembly by 25 Å, resulting in helicity (Figure 6 c).

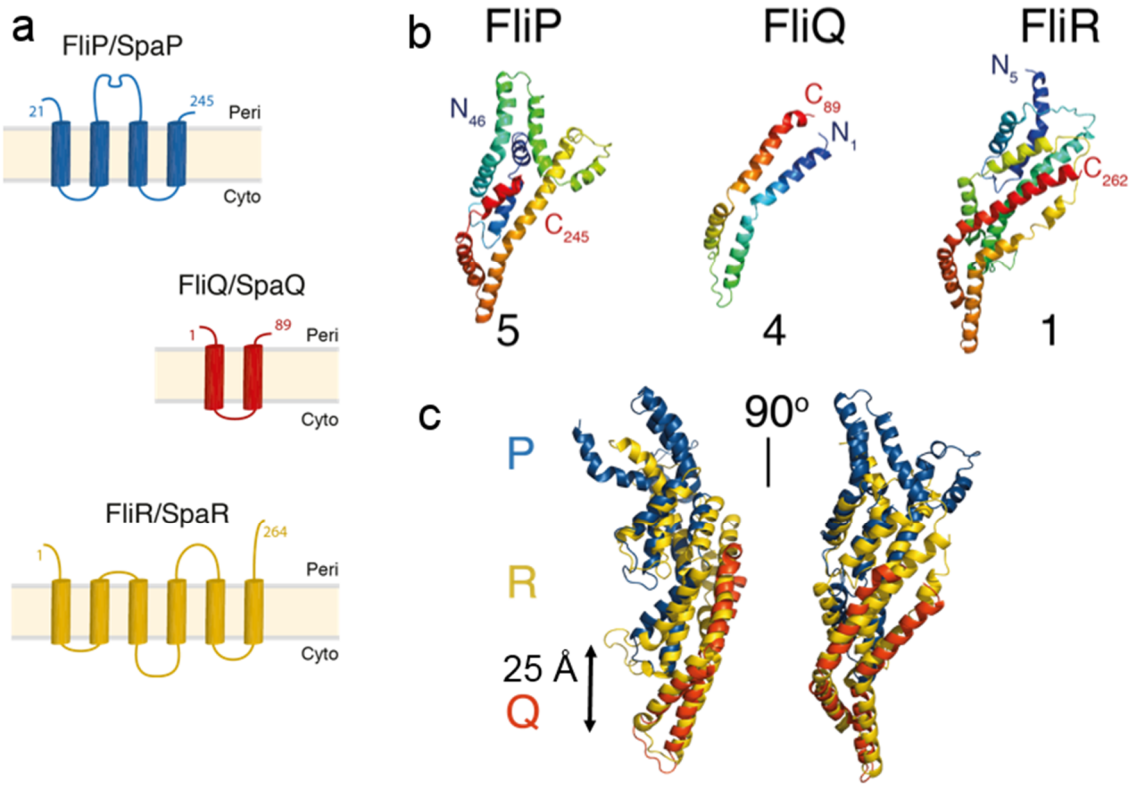

Figure 6: The membrane protein character with TMDs is still visible in the SpaPQR complex.
(a) Schematic view of the transmembrane domains of export apparatus proteins. SpaR as a fusion of SpaP and SpaQ is illustrated here Peri: periplasm, Cyto: cytoplasm.
(b) Homology model of flagellar homologs FliP, FliQ and FliR. TMDs are still recognisable as twisted alpha-helical stretches. N-terminus and C-terminus marked.
(c) Side views on homology model of the assembled PRQ complex.
(Samuel Wagner, personal communication 2020)

1.5 Genetic conservation and regulation of the export apparatus

When comparing the export apparatus of the flagellar and SPI-1 T3SS, several aspects stand out. At first, it becomes apparent that in the SPI-1 T3SS there is no counterpart to the flagellar chaperone FliO (Fabiani et al. 2017). Flagellar genes in different species often lie in clusters, but show different orders and distances between them (Macnab 2004). The genes coding for the injectisome are usually located in pathogenicity islands on virulence plasmids or on the genome and are more closely related than their corresponding genes in flagella (Naum et al. 2009).

Gophna *et al*. performed phylogenetic analyses of the individual export apparatus proteins exemplarily on the SpaP sequence (respective their homologues) of 19 bacterial species and the FliP sequence in flagella for 23 species. Similarly, SpaQ and FliQ analyses were performed in 20 and 25 species, respectively. With regard to *S. enterica*, these analyses showed its greatest similarity to *E. coli*, followed by *Shigella flexneri*, *Yersinia enterocolitica* and other species such as *Pseudomonas aeruginosa*. Flagellar proteins showed greater phylogenetic discrepancies (Gophna et al. 2003). Comparison of the single particle cryo-EM analyses revealed a 33% identical structure of FliPQR in flagella of *S*. Typhimurium (homologue to SpaPQR) and the corresponding proteins Spa24, Spa9 and Spa29 in *Shigella* (Johnson et al. 2019).

Flagellar and virulence-associated T3SS probably share a common ancestor. Deletions and newly acquired genes subsequently led to the loss of motility and the acquisition of the specific export capabilities of today's T3SS (Abby and Rocha 2012). Compared to other pathogenicity islands of *E. coli* or *Yersinia*, SPI-1 shows a significantly longer residency time in the host genome of several tens of millions of years (Lerminiaux et al. 2020). The export apparatus is still highly conserved.

A good overview of the conservation of the export apparatus and other components of the T3SS also in plant pathogens can be found in the article by Lerminiauux *et al.* (2020). I have limited the overview to the export apparatus of human pathogenic species (Figure 7).

In *E. coli* the *spaS* equivalent *flhB* is located at a different site in the genome, but *fliP*, *fliQ* and *fliR* show high conservation. In *Yersinia* the genes are located on virulence plasmids, but as in SPI-1, they are also organized in an operon.

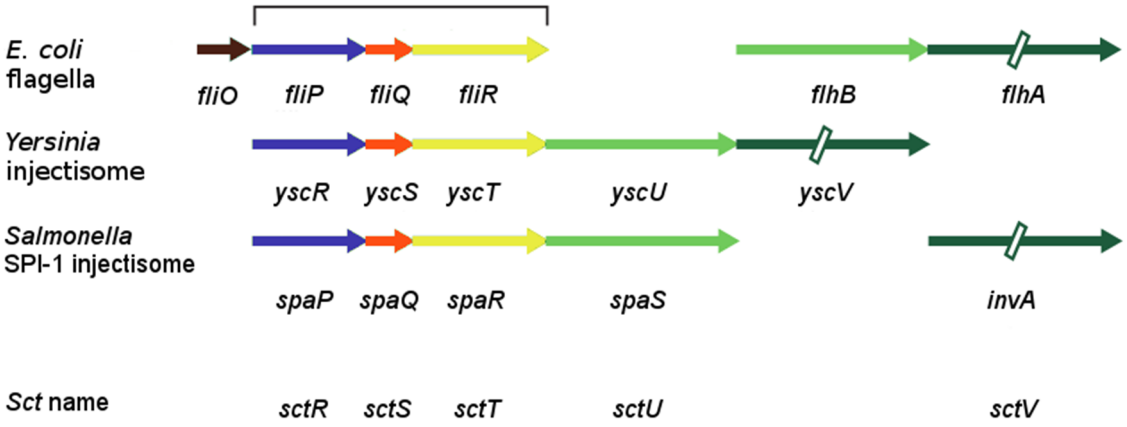

Figure 7: Comparison of the genetic organization of *spaPQRS* and their homologs in flagella (*E. coli*) and *Yersinia*.
The genes of the export apparatus are labeled according to species and additionally according to the unified nomenclature (*Sct* name). The bracket indicates high genetic conservation.

Sukhan *et al.* could show that all five genes of the export apparatus are essential for a functional T3SS (2001). However, a deletion of *invA* or *spaS* barely influences the assembly of the other components of the export apparatus (Wagner et al. 2010). The application of cryo electron microscopy allows even more detailed statements about the structure of the assembled complex. If *invA* is deleted, the assembly of the other export apparatus proteins still equals the wild type. In a Δ*spaP,* Δ*spaQ* or *ΔspaR* strain, the assembly resembles a knockout of the entire export apparatus.

For this reason, a changed order of the genes is especially interesting for *spaP*, *spaQ* and *spaR*.

The work of Dandekar *et al*. also reports on physical interactions of proteins encoded by highly conserved genes (1998). This supports the hypothesis that the highly conserved order of genes has a functional significance.

Since the gene dosage of *spaPQRS* on the polycistronic mRNA is 1:1:1:1 but the stoichiometry in the final export apparatus is 5:4:1:1, the question arises which mechanisms compensate this imbalance.

One possibility would be the differential regulation of the efficiencies of the Shine-Dalgarno (SD) sequences. The SD sequence is a short base sequence located generally 7-8 bp upstream of the start codon, which facilitates ribosome binding

and the start of translation. The ideal sequence is aggagg, but variations are often observed. In bacteria, several genes exist under one promoter, each having its own SD. In some cases, the reading quantity is directly related to the upstream gene. This principle, called translational coupling, has been described for *spaQ* and *spaR* (Zhou 2017). In the case of *spaQ* and *spaR* the SD of *spaR* is still within *spaQ*. The coding sequences of *spaR* and *spaS* even overlap to a small extent. In these cases, it is likely that the ribosome does not detach but reads through continuously.

Another possibility would be differential translation as a result of the distinct mRNA structure, as clarified below.

1.6 mRNA structure

Related to the gene sequence, but even independently of that, the mRNA structure itself can have an influence on translation efficiency (Li 2015): By base pairing and subsequent folding, regulatory elements of the primary RNA can become difficult to access (John E.G. McCarthy and Claudio Gualerzi 1990). Possibly, the stem-loop structure of the mRNA makes it more difficult for the ribosome to bind to the SD, as shown by Zhou. By introducing point mutations that melted the mRNA structure of *spaQ*, the author was able to induce the overexpression of SpaR (2017). The structure predicted by the RNAfold-prediction tool ViennaRNA Web Services supports these findings (Figure 8). Paroll has suspected that *spaQ* apparently performs a regulatory function on *spaR* (2016). This will also be examined in the present study.

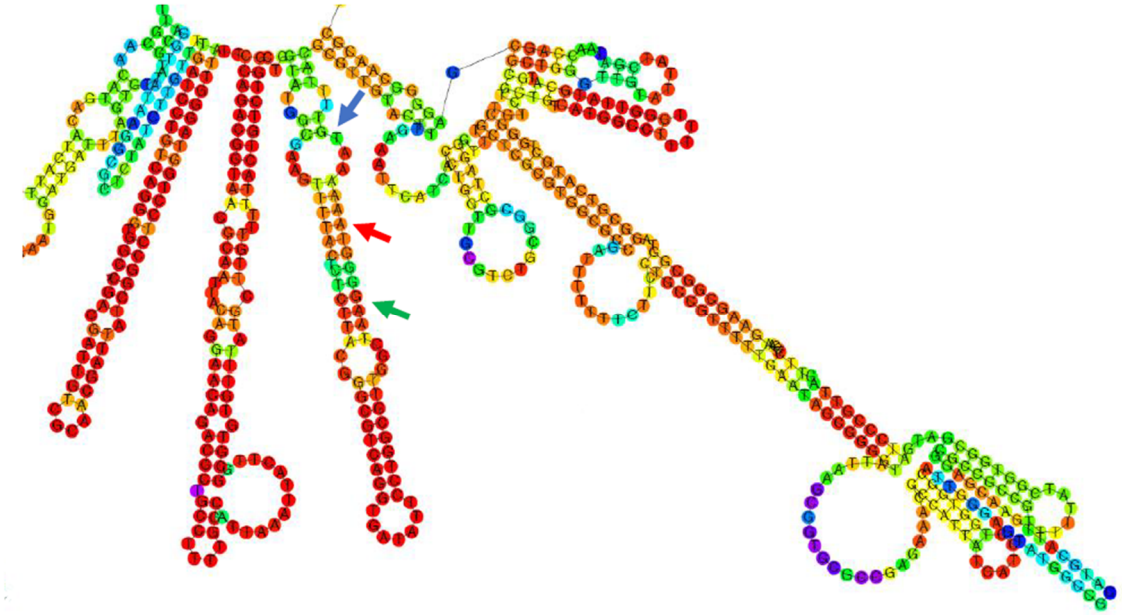

Figure 8: Predicted mRNA folding of *spaR* and *spaQ* and possible topological difficulties.
The folding of the mRNA may impede the attachment of the ribosome to the SD of *spaR*, thus enabling *spaQ* to perform a regulatory function on the translation of *spaR*. Green arrow: predicted SD of *spaR*, red arrow: stop codon of *spaQ*, blue arrow: start codon of *spaR.* (Source: Zhou 2017)

1.7 Objectives

The goal of this study is to determine the relevance of the strict conservation of the gene order of *spaP*, *spaQ* and *spaR* for the assembly and function of the T3SS by assessing transcription, translation, assembly and secretion.

The conserved gene order does not match the assembly order. Is this relevant and can efficiency be improved if the gene order is identical to the assembly order? Are there differences observed in case of permutation of the gene order? If yes, which conclusions regarding gene interaction can be drawn? If, upon permutation, the assembly is defective, it would be interesting and meaningful to investigate at which step the error occurs. This is specifically what we tested by permutating the gene order.

2 Material and Methods

All materials were purchased from AppliChem, Beckmann, Eppendorf, Eurofins Genomics, Life Technologies, neoLab, ROTH, Sarstedt, SERVA, Sigma-Aldrich, Star Lab, Thermo Fisher or VWR.

2.1 Antibodies, buffers, media

Table 1: List of antibodies used

Antibody	Clonality	Dilution	Origin	Order	Source
α-FLAG, M2	monoclonal	1:10 000	mouse	primary	Sigma
α-Mouse DyLight 800	polyclonal	1:10 000	goat	secondary	ThermoFisher

Table 2: Contents of buffers and media

Name	Description
Media for bacterial culture	
Luria broth (LB) agar medium	4.5 g agar and 6 g LB Lennox were added to 300 ml H_2O and autoclaved before use.
LB medium	5 g NaCl, 5 g yeast extract and 10 g tryptone were dissolved in 1 l H_2O and autoclaved before use.
LB - 0.3M NaCl medium	12.5 g NaCl, 5 g yeast extract and 10 g tryptone were dissolved in 1 l H_2O and autoclaved before use.
super optimal broth (SOB) medium	40 g bacto-tryptone, 0.373 g KCl, 1 g NaCl and 10 g yeast extract were dissolved in 2 l H_2O and autoclaved. Sterile filtered (0.22 µm pore size), $MgCl_2$ and $MgSO_4$ solutions were added to a final concentration of 10 mM.
SOC medium	20 ml sterile filtered (0.22 µm pore size) 1 M glucose were added to 1 l SOB medium.
Stock medium	63 g glycerol and 10 g peptone were dissolved in 500 ml H_2O and autoclaved before use.
Reagents for cloning	
Gibson master mix	0.2 µl T5 exonuclease, 6.25 µl Phusion DNA polymerase, 50 µl *Thermus aquaticus* (*Taq)* DNA Ligase and 100 µl 5× ISO mix (containing 300 µl 1 M Tris-HCl, 30 µl 1 M $MgCl_2$, 60 µl 10 mM dNTP Mix, 30 µl 1 M DTT,

	150 mg PEG 8000, 30 µl 100 mM NAD and 600 µl H_2O) were mixed with 218.6 µl H_2O.
Buffers for crude membranes	
Buffer K	50 mM TEA, 250 mM sucrose and 1 mM ethylenediaminetetraacetic acid (EDTA) were dissolved in 500 ml H_2O. pH was adjusted to 7.5 using acetic acid.
Buffer K with additives	750 µl buffer K mixed with 1:100 protease inhibitor from 100× stock, 1:1000 lysozyme from 10 µg / ml stock, 1:1000 $MgCl_2$ from 1 M stock, 1:500 EDTA from 0.5 M stock, 1:1000 DNase from 10 µg / ml stock
phosphate buffered saline (PBS) buffer (10x)	80 g NaCl, 2 g KCl, 14.4 g Na_2HPO_4 and 2.4 g KH_2PO_4 were dissolved in 1 l H_2O. pH was adjusted to 7.4 using NaOH.
Buffers for Blue Native PAGE (BN PAGE)	
BN PAGE loading buffer	25 mg Coomassie Brilliant Blue G-250 were dissolved in 450 µl 250 mM aminocaproic acid with 25% (v/v) glycerol.
Anode buffer (10×)	52.3 g Bis-Tris were dissolved in 500 ml H_2O. The buffer was diluted 1:10 with deionized H_2O before use.
Cathode buffer I (10×)	44.79 g tricine, 15.69 g Bis-Tris and 1 g Coomassie Brilliant Blue G-250 were dissolved in 500 ml H_2O and mixed for at least six hours at 4 °C. The buffer was diluted 1:10 with deionized H_2O before use.
Cathode buffer II (10×)	44.79 g tricine and 15.69 g Bis-Tris were dissolved in 500 ml H_2O. 20 ml of cathode buffer I were mixed with the equal volume of cathode buffer II (10×) and filled up to 210 ml with deionized H_2O before use.
Buffers for Western Blot	
SB buffer (4×)	10 mg bromophenol blue, 5 ml 80% (v/v) glycerol, 1.6 g sodium dodecyl sulfate (SDS) and 10 ml 0.5 M Tris-HCl were filled up with H_2O to a final volume of 16 ml. The buffer was diluted 1:4 with deionized H_2O and 5% (v/v) β-mercaptoethanol were added before use.
SDS Running buffer	144 g glycine, 10 g SDS and 30 g Tris base were dissolved in 1 l H_2O.
Tris-buffered saline (TBS) buffer (10×)	84 g NaCl and 30 g Tris base were dissolved in 1 l H_2O. pH adjustment to 8.0 with HCl.
TBS-T buffer	0.05% (v/v) Tween20 were added to TBS.
Transfer buffer (10×)	144 g glycine, 2.5 g SDS and 30 g Tris base were dissolved in 1 l H_2O. Before use, the buffer was diluted 1:10 in H_2O and methanol was added to a final concentration of 10% (v/v).

2.2 Culture conditions

For cloning procedures, *Escherichia coli (E. coli)* and *S*. Typhimurium were grown in Luria broth (LB) medium. For the SipA-NanoLuc-assay and crude membrane preparation, *S*. Typhimurium was grown in LB medium supplemented with 0.3 M NaCl (Gibson et al. 1988).

2.2.1 Bacterial growth and storage

The tubes were shaken at 37 °C and at 180 revolutions per minute (rpm) in the incubator. The required antibiotics were added in the following concentrations:

Table 3: Concentrations of the antibiotics used

Antibiotic	Final concentration (µg/ml)
Kanamycin	25
Streptomycin	50
Tetracycline	12.5

Growth on solid media containing appropriate antibiotics took place at 37 °C. For short-term storage, the bacteria were stored on agar plates at 4 °C, for long-term storage they were frozen in solution with stock medium (Table 2) at -80 °C.

2.2.2 Protein overexpression induced with L-rhamnose

To selectively increase protein expression for experimental purposes, low copy number L-rhamnose-inducible plasmid pTACO10 (pT10) were used (Wagner et al. 2010).

Bacteria were grown over night in 3 ml LB with antibiotics. For crude membranes, the optical density at 600 nm (OD_{600}) was measured and the bacterial culture was

backdiluted in 10 ml LB + NaCl with antibiotics to a final OD of 0.05. In preparation for the SipA luciferase assay, bacteria were backdiluted in a new tube containing 2 ml LB + NaCl medium and antibiotics to a final OD of 0.1. After three hours growth in the incubator under the conditions described in 2.2.1, rhamnose at a final concentration of 0.1 mM was added to induce protein overexpression from the pT10 plasmid.

2.3 Cloning procedures

For cloning, three different polymerase chain reaction (PCR)-based methods were used. Gibson Assembly was used to rearrange whole genes, the Megaprimer method to insert or delete gene segments and QuikChange to introduce point mutations (see 2.6).

2.3.1 Gibson Assembly

Gibson Assembly (Gibson et al. 2009) is an isothermal method used for molecular cloning. It allows joining of two or more DNA fragments. Gibson primers are designed in a way that half of the base sequence is complementary to the template DNA and the other half forms an overhang that is complementary to the product from a second PCR. The resulting amplification products are then ligated in the next step.

A 20-40 base pairs (bp) overlap was added via PCR with a specific primer. In a next step, 1 µl of each fragment was added to a Gibson reaction mix, containing buffer, exonuclease, DNA polymerase and DNA ligase and incubated for 30 minutes at 50 °C. Chemically competent *E. coli* were transformed with the reaction product using standard procedure (New England Biolabs 2020). Colony PCR was used to identify clones with the inserts of the correct length. These clones were grown over night in 3 ml LB medium. The following day, plasmids

were extracted with QIAprep Spin Miniprep Kit from QIAGEN and stored at -20 °C.

2.3.2 QuikChange site-directed mutagenesis

In order to be able to investigate the effect of the SpaQ remnant protein, a stop codon was inserted as a point mutation using QuikChange mutagenesis (Agilent 2020) .
Primers were designed with a length of 47 bp carrying the desired point mutation in the middle, flanked by sections rich in guanine and cytosine bases in both directions.

A PCR reaction mix with KOD Polymerase was set up as described in Table 4.

Table 4: QuikChange PCR setup

Reagent	Volume added to PCR reaction
10× KOD Reaction Buffer	5 µl
2 mM dNTPs	5 µl
forward and reverse primer	1.25 µl each
KOD DNA Polymerase	0,5 µl
25 mM $MgSO_4$	4 µl
double deionized water (ddH_2O)	30 µl
template DNA	3 µl

After amplification in the thermocycler, 1 µl of DpnI was added and incubated at 37 °C for one hour. The restriction enzyme DpnI cuts methylated DNA and ensures that the template DNA is digested and the PCR product remains. Heat shock transformation into *E. coli* strain NEB5α was performed as described in 2.3.1.

2.3.3 Megaprimer mediated mutagenesis

This method was used to transfer individual gene segments of up to 74 bp from one construct to another. This requires two PCRs, with the product of the first PCR serving as primer in the second. (Casali and Preston 2003)

In a first step, the desired gene segment was amplified with two suitable primers in a PCR. DpnI digestion was then performed (see 2.3.2) and 5 µl of the PCR product were used as Megaprimer in a second PCR (setup see Table 5).

Table 5: Megaprimer PCR setup

Reagent	Volume added to PCR reaction
5× Phusion HighFidelity buffer	10 µl
10 mM dNTPs	1 µl
Megaprimer	5 µl
Phusion DNA Polymerase	1 µl
dimethyl sulfoxide (DMSO)	1.5 µl
ddH_2O	29.5 µl
template DNA	2 µl

Again, DpnI digestion and purification were performed and the *E. coli* strain NEB5α was transformed with the PCR product as described in 2.3.1.

2.4 Blue-Native (BN)- and Sodium dodecyl sulfate (SDS) - polyacrylamide gel electrophoresis (PAGE)

The BN PAGE method is used to detect protein complexes while maintaining their protein quaternary structure. The cytoplasmic components are too unstable for the BN PAGE, but the needle complex (NC) consisting of base, needle and needle tip can be analyzed using this technique (Wagner et al. 2010). The dye Coomassie Brilliant blue G-250 binds to hydrophobic surfaces of membrane proteins that have been solubilized with detergent. This confers an electric charge to the proteins and forms the basis for electrophoretic complex separation on a gradient gel (Schägger and von Jagow 1991).

In order to be able to analyze the individual proteins quantitatively and independently of their complexes, SDS was used as a stronger detergent (Laemmli 1970). The proteins are extracted from the membrane and retain only their primary structure and parts of the secondary structure. Again, the separation is carried out electrophoretically according to size and charge.

2.4.1 Crude Membranes

In a first step, the proteins must be overexpressed and isolated from the membrane. Bacterial cultures were prepared and induced as described in 2.2.2. After five hours in the incubator, the OD_{600} was measured and 8 ODU were transferred to a 15 ml tube. From now on, all steps were performed on ice and centrifugation was done at 4 °C. The tubes were centrifuged at 6000 × *g* for 2 minutes. The supernatant was discarded, the pellet was resuspended in 1.5 ml PBS and the centrifugation step was repeated. After aspiration of the supernatant with a vacuum pump, the samples were stored at -80 °C if not analyzed immediately.

The pellet was resuspended in 750 µl buffer K with additives (Table 2) and added to 2 ml screw cap tubes filled with 0.5 ml glass beads. The samples were incubated on ice for 30 minutes and then lysed by a bead mill for 2 minutes. The tubes were centrifuged at 1000 × *g* for 1 minute and the supernatant was transferred to a fresh 1.5 ml tube. 1 ml of cold buffer K without additives was added to the beads and the centrifugation step was repeated. The supernatant was then transferred to the same 1.5 ml tube and the samples were centrifuged at 10 000 × *g* for 10 minutes. Afterwards, the supernatant was transferred to an ultracentrifugation tube and the samples were centrifuged at 120 000 × *g* for 50 minutes using an ultracentrifuge with a TLA-55 rotor. Afterwards the supernatant was completely aspirated and the pellets were resuspended with 90 µl PBS. After addition of 10 µl 10% (w/v) lauryl maltose neopentyl glycol (LMNG) solution, the samples were solubilized at 4 °C for 1 h inside a Thermomix device shaking at 500 rpm. The samples were then centrifuged at 20 000 × *g* for

30 minutes. 45 µl of the supernatant were transferred to a new tube in order to proceed with BN PAGE and 30 µl were used for SDS PAGE.

2.4.2 BN PAGE

The Invitrogen™ NativePAGE™ 4-16% Protein Gel was set up according to manufacturer instructions, and anode buffer and cathode buffer were filled into the respective chambers.

5 µl of BN PAGE loading buffer was added to each sample, and 20 µl were then loaded into each gel pocket. 8 µl of Native Mark™ unstained protein standard was used as a size reference. The electrophoresis ran at 130 V for 65 minutes, then the cathode buffer I was replaced by cathode buffer II and voltage was increased to 300 V for 3.5 h. After the run, the gel was equilibrated in SDS running buffer for 30 minutes.

Wet Blot was done as described below (see 2.4.4) but after the transfer onto a membrane, the membrane was washed several times with 100% methanol to remove blue Coomassie residuals before the blocking step. A standard Western Blot protocol was then carried out.

2.4.3 SDS-PAGE of whole bacteria

Whole cells were pelleted, resuspended in 75 µl of 1× solubilization buffer (Table 2) and incubated at 50 °C for 10 minutes. Afterwards, the samples were vortexed for 40 seconds and 15 µl were loaded on SERVA*Gel*™ TG PRiME™ 8-16% electrophoresis gel. The protein ladder used as size reference was Precision Plus™ Protein All Blue standards.

The electrophoresis ran for 15 minutes at 100 V followed by 70 minutes at 210 V.

2.4.4 Western Blotting

Transfer from the gel onto a polyvinylidene difluoride membrane by wet blotting was done using an electrophoretic chamber filled with transfer buffer at 25-30 V for four hours. To block unspecific binding sites on the membrane, 5% (w/v) milk in Tris-buffered saline (TBS) buffer was used for one hour. Afterwards, the membrane was washed with TBS supplemented with 0.05% (v/v) Tween20 (TBS-T) buffer. Incubation with primary antibody (Table 1) was done for one hour in 10 ml TBS and washed three times for fifteen minutes with TBS-T. The secondary antibody (Table 1) was then added to 10 ml TBS and incubated with the membrane for one hour. Afterwards, the membrane was washed three times for fifteen minutes with TBS-T again. The membrane was then transferred to TBS buffer and scanned using LI-COR reader.

2.5 SipA luciferase-based secretion assay

This method is used to estimate the secretion capability of the T3SS. The luciferase NanoLuc is fused C-terminally to the effector SipA (Westerhausen et al. 2019). After growth and rhamnose induction in LB + NaCl, the bacteria are pelleted. The supernatant is mixed with a substrate containing furimazine. This is converted by luciferase to furimamide, which emits light that can be quantified.

Rhamnose induction has been done as described in 2.2.2, and after five hours of growth, 0.5 ODU were transferred into a 1.5 ml tube, centrifuged at 10 000 × *g* for 2 minutes. 25 µl of the supernatant were transferred to a white 384-well plate (MaxiSorp). NanoLuc life substrate was prepared according to manufacturer's instructions and 25 µl were added to each well. After exactly 5 minutes of incubation, the luminescence signal was analyzed by TECAN microplate reader.

2.6 Tables of materials

Table 6: List of bacteria used

Name	Species	Genotype
NEB5α	*Escherichia coli*	*fhuA2Δ (argF-lacZ)U169 phoA glnV44 ϕ80Δ(lacZ)M15 gyrA96 recA1 relA1 endA1 thi-1 hsdR17* (New England Biolabs 2020b)
SB300	*Salmonella enterica subspecies* enterica *serovar Typhimurium*	wild type
SB1903	*Salmonella enterica*	SB300, Δ*spaQ*, *flhD::tet*
SB1904	*Salmonella enterica*	SB300, Δ*spaR*, *flhD::tet*
SB2000	*Salmonella enterica*	SB300, Δ*spaQ,* $SpaP_{84}^{FLAG}$, *flhD::tet*
SB2001	*Salmonella enterica*	SB300, Δ*spaR,* $SpaP_{84}^{FLAG}$, *flhD::tet*
SB2009	*Salmonella enterica*	SB300, Δ*spaQ,* $SpaR_{251}^{FLAG}$, *flhD::tet*
SB2013	*Salmonella enterica*	SB300, Δ*spaQ,* $SpaS_{N258A356}^{FLAG}$, *flhD::tet*
SB2014	*Salmonella enterica*	SB300, Δ*spaR,* $SpaS_{N258A356}^{FLAG}$, *flhD::tet*
MIB4592	*Salmonella enterica*	SB300, Δ*spaPQRS*, SipA-NL, *flhD::tet*

Table 7: List of primers used

Primer name	Sequence (5’ to 3’)
gib_behind_spaP234_r	aatgtccatatactgtaatatcaatcc
gib_infront_spaQ_f	catcattacgagacgggatag
gib_pT12_FLAG_r	ctctcatccgccaaaacagccaagcttcatttgtcatcgtcatccttgtaatc
gib_pT12_spaP_f	gaaattcaggaggaattcaccatggggaatgatatctcattaattg
gib_pT12_spaS_r	catccgccaaaacagccaagcttcaatgccgtacctcgttttc
gib_pt12n_spaR_f	ctttttagactggtcgtaatgaacgttggctaaggggtaaaaaatg
gib_pT12nSpaQ_f	ctttttagactggtcgtaatgaattacgagacgggatagttaaatg
gib_pT12upoSpaP_SpaQ_r	attccccatggtgaattcctcctgaatttcttacccctagccaacgccag
gib_pT12upoSpaP_SpaR_r	attccccatggtgaattcctcctgaatttcttattcgaggacatgcgtcgc
gib_SpaP164_f	ttttatctttatttgccctttgtcgtc
gib_spaP234_spaR_f	gtctaagggattgatattacagtatatggacattaaggggtaaaaaatgttttacgcg
gib_spaQ_spaR_f	cctggcgttggctaaggggtaaaaaatgttttacgcg
gib_spaQ_spaR_r	catccatttaactatcccgtctcgtaatgatgttattcgaggacatgcgtcgc
gib_spaR_spaQ_f	gggcgacgcatgtcctcgaataaattacgagacgggatagttaaatgg
gib_spaS_spaP_r	catgcgtcgcccctcgctcgtaatgatgtcatgttgcaatgtccatatac
gib_uni_pT12_f	agcttggctgttttggcggatg
gib_uni_pT12_r	ggtgaattcctcctgaatttc
gib_uni_pT12noSD_r	ttcattacgaccagtctaaaaag
gib_uni_pT12upo_f	gaaattcaggaggaattcaccatg
gib_uni_spaQ_r	ttacccttagccaacgccag
gib_uni_spaR_r	ttattcgaggacatgcgtcgc
gib_uni_spaS272_f	ttgatgccgattccgatgatc
gib_uni2_spaS_f	agcgaggggcgacgcatg
prha_seq_r	gctacggcgtttcacttctg

spaO_seq_r	aacgaaacaggttcctgacg
SpaQ_seq_r2	aatgccaccaggatgataatg
spaP_seqr	ctaccaggaggccgataatc
SpaP45_seq_f	taacgccctgggattacagc
spaPA223KT224G_QC_f	gtctaagggattgatattacagtatatggacattaaggggtgacatcattacgagacgggata
spaPA223KT224G_QC_r	tatcccgtctcgtaatgatgtcacccctaatgtccatatactgtaatatcaatcccttagac
SpaQ_remnant_PR_M1K_QC_f	cattacgagacgggatagttaaaaggatgatttagtgtttgcaggtg
SpaQ_remnant_PR_M1K_QC_r	cacctgcaaacactaaatcatccttttaactatcccgtctcgtaatg
SpaQ_seq_r	aatgccaccaggatgataatg
SpaR_seq_r	aaatgagccatacgacaccag
SpaR207_seq_f	ttattgtcgcgctttgctcc
spaS_seqf	gacaatgtactgcgactctc

Table 8: List of plasmids used

Name	Insert	Description
pSB3398	none	(Wagner et al. 2010)
pSB3704	*spaP*^{84FLAG}*QRS*	(Wagner et al. 2010)
pMIB5022	*spaPQR*^{251FLAG}*S*	(Wagner et al. 2010)
pMIB6089	*spaPQRS*$_{N258A}$^{356FLAG}	(Wagner et al. 2010)
pMIB6610	*spaP*^{84FLAG}*Q*$_{261+1}$*::ins20R*[1]	(Zhou 2017)
pMIB6666	*spaPR*^{251FLAG}*Q*	(Zhou 2017)
pMIB6670	*spaP*^{84FLAG}$_{741+3}$*::ins20QR*[2]	(Zhou 2017)
pMIB7001, SpaP^^{L}RS	*spaPQ*$_{\Delta 24-231}$*RS*	Made by Gibson assembly of PCR products of the following two primer/template pairs: 1. Insert: gib_pT12_spaP_f + gib_pT12_spaS_r from SB1903 chromosomal DNA; 2. Plasmid: gib_uni_pT12_f + gib_uni_pT12_r from pSB3398 (pT10).
pMIB7002, SpaP^{FLAG}^^{L}RS	*spaP*^{84FLAG}*Q*$_{\Delta 24-231}$*RS*	Made by Gibson assembly of PCR products of the following two primer/template pairs: 1. Insert: gib_pT12_spaP_f + gib_pT12_spaS_r from SB2000 chromosomal DNA; 2. Plasmid: gib_uni_pT12_f + gib_uni_pT12_r from pSB3398 (pT10).

[1] The 20 bp insert is tatgatatattcagatcgcg
[2] The 20 bp insert is tttgatataaaaggggtgaa, including the SD of *spaR* (aagggg)

pMIB7003, SpaP$^{\wedge L}$R^{FLAG}S	*spaPQ$_{\Delta 24\text{-}231}$R^{251FLAG}S*	Made by Gibson assembly of PCR products of the following two primer/template pairs: 1. Insert: gib_pT12_spaP_f + gib_pT12_spaS_r from SB2009 chromosomal DNA; 2. Plasmid: gib_uni_pT12_f + gib_uni_pT12_r from pSB3398 (pT10).
pMIB7004, SpaP$^{\wedge L}$RS^{FLAG}	*spaPQ$_{\Delta 24\text{-}231}$RS$_{N258A}$^{356FLAG}*	Made by Gibson assembly of PCR products of the following two primer/template pairs: 1. Insert: gib_pT12_spaP_f + gib_pT12_FLAG_r from SB2013 chromosomal DNA; 2. Plasmid: gib_uni_pT12_f + gib_uni_pT12_r from pSB3398 (pT10).
pMIB7005, SpaPQS	*spaPQR$_{\Delta 43\text{-}735}$S*	Made by Gibson assembly of PCR products of the following two primer/template pairs: 1. Insert: gib_pT12_spaP_f + gib_pT12_spaS_r from SB1904 chromosomal DNA; 2. Plasmid: gib_uni_pT12_f + gib_uni_pT12_r from pSB3398 (pT10).
pMIB7006, SpaP^{FLAG}QS	*spaP^{84FLAG}QR$_{\Delta 43\text{-}735}$S*	Made by Gibson assembly of PCR products of the following two primer/template pairs: 1. Insert: gib_pT12_spaP_f + gib_pT12_spaS_r from SB2001 chromosomal DNA; 2. Plasmid: gib_uni_pT12_f + gib_uni_pT12_r from pSB3398 (pT10).

pMIB7007, SpaPQS^{FLAG}	*spaPQR$_{\Delta 43\text{-}735}$S$_{N258A}$^{356FLAG}*	Made by Gibson assembly of PCR products of the following two primer/template pairs: 1. Insert: gib_pT12_spaP_f + gib_pT12_FLAG_r from SB2014 chromosomal DNA; 2. Plasmid: gib_uni_pT12_f + gib_uni_pT12_r from pSB3398 (pT10).
pMIB7008, SpaR^{FLAG}PQS	*spaR^{251FLAG}PQR$_{\Delta 43\text{-}735}$S*	Made by Gibson assembly of PCR products of the following two primer/template pairs: 1. Insert: gib_pT12n_spaR_f + gib_pT12upoSpaP_SpaR_r from SB2009 chromosomal DNA; 2. Plasmid: gib_uni_pT12upo_f + gib_uni_pT12noSD_r from pMIB7005 (pT10).
pMIB7009, SpaRP^{FLAG}QS	*spaRP^{84FLAG}QR$_{\Delta 43\text{-}735}$S*	Made by Gibson assembly of PCR products of the following two primer/template pairs: 1. Insert: gib_pT12n_spaR_f + gib_pT12upoSpaP_SpaR_r from SB1903 chromosomal DNA; 2. Plasmid: gib_uni_pT12upo_f + gib_uni_pT12noSD_r from pMIB7006 (pT10).

pMIB7010, SpaRPQS^{FLAG}	*spaRPQR$_{\Delta 43\text{-}735}$S$_{N258A}$^{356FLAG}*	Made by Gibson assembly of PCR products of the following two primer/template pairs: 1. Insert: gib_pT12n_spaR_f + gib_pT12upoSpaP_SpaR_r from SB1903 chromosomal DNA; 2. Plasmid: gib_uni_pT12upo_f + gib_uni_pT12noSD_r from pMIB7007 (pT10).
pMIB7011, SpaP$^{\wedge S}$R^{FLAG}QS	*spaP$_{\Delta 666\text{-}Q252}$R^{251FLAG}QS*	Made by Gibson assembly of PCR products of the following two primer/template pairs: 1. Insert: gib_SpaP234_spaR_f + gib_SpaQ_SpaR_r from SB2009 chromosomal DNA; 2. Plasmid: gib_infront_SpaQ_f + gib_behind_SpaP234_r from pMIB7005 (pT10).
pMIB7012, SpaP$^{FLAG\wedge S}$RQS	*spaP^{84FLAG}$_{\Delta 666\text{-}Q252}$RQS*	Made by Gibson assembly of PCR products of the following two primer/template pairs: 1. Insert: gib_SpaP234_spaR_f + gib_SpaQ_SpaR_r from SB1903 chromosomal DNA; 2. Plasmid: gib_infront_SpaQ_f + gib_behind_SpaP234_r from pMIB7006 (pT10).

pMIB7013, SpaP$^{\wedge S}$RQS^{FLAG}	*spaP$_{\Delta 666Q252}$RQS$_{N258A}$^{356FLAG}*	Made by Gibson assembly of PCR products of the following two primer/template pairs: 1. Insert: gib_SpaP234_spaR_f + gib_SpaQ_SpaR_r from SB1903 chromosomal DNA; 2. Plasmid: gib_infront_SpaQ_f + gib_behind_SpaP234_r from pMIB7007 (pT10).
pMIB7014, SpaQP$^{\wedge L}$RS	*spaQPQ$_{\Delta 24-231}$RS*	Made by Gibson assembly of PCR products of the following two primer/template pairs: 1. Insert: gib_pT12n_SpaQ_f + gib_pT12upoSpaP_SpaQ_r from SB1904 chromosomal DNA; 2. Plasmid: gib_uni_pT12upo_f + gib_uni_pT12noSD_r from pMIB7001 (pT10).
pMIB7015, SpaQP^{FLAG} $^{\wedge L}$RS	*spaQP^{84FLAG}Q$_{\Delta 24-231}$RS*	Made by Gibson assembly of PCR products of the following two primer/template pairs: 1. Insert: gib_pT12n_SpaQ_f + gib_pT12upoSpaP_SpaQ_r from SB1904 chromosomal DNA; 2. Plasmid: gib_uni_pT12upo_f + gib_uni_pT12noSD_r from pMIB7002 (pT10).

pMIB7016, SpaQP^LR^{FLAG}S	*spaQPQ$_{Δ24-231}$R^{251FLAG}S*	Made by Gibson assembly of PCR products of the following two primer/template pairs: 1. Insert: gib_pT12n_SpaQ_f + gib_pT12upoSpaP_SpaQ_r from SB1904 chromosomal DNA; 2. Plasmid: gib_uni_pT12upo_f + gib_uni_pT12noSD_r from pMIB7003 (pT10).
pMIB7017, SpaQP^LRS^{FLAG}	*spaQPQ$_{Δ24-231}$RS$_{N258A}$^{356FLAG}*	Made by Gibson assembly of PCR products of the following two primer/template pairs: 1. Insert: gib_pT12n_SpaQ_f + gib_pT12upoSpaP_SpaQ_r from SB1904 chromosomal DNA; 2. Plasmid: gib_uni_pT12upo_f + gib_uni_pT12noSD_r from pMIB7004 (pT10).
pMIB7018, spaQP^{FLAG}^SRS	*spaQP^{84FLAG}$_{Δ666-Q252}$RS*	Made by Megaprimer from Plasmid pMIB7016. Megaprimer derived from pMIB7012 using SpaP45_seq_f + SpaQ_seq_r.
pMIB7019, SpaQP^SR^{FLAG}S	*spaQP$_{Δ666-Q252}$R^{251FLAG}S*	Made by Megaprimer from Plasmid pMIB7016. Megaprimer derived from pMIB7012 using gib_SpaP164_f + SpaQ_seq_r.
pMIB7020, SpaQP^SRS^{FLAG}	*spaQP$_{Δ666-Q252}$RS$_{N258A}$^{356FLAG}*	Made by Megaprimer from Plasmid pMIB7017. Megaprimer derived from pMIB7012 using gib_SpaP164_f + SpaQ_seq_r.

pMIB7041, SpaP$^{FLAG\text{^}S}$RS	*spaP$^{84FLAG}{}_{\Delta 666\text{-}Q252}$RS*	Made by Megaprimer from Plasmid pMIB7015. Megaprimer derived from pSB3704 using SpaP45_seq_f + SpaQ_seq_r.
pMIB7042, SpaP$^{\text{^}S}$R^{FLAG}S	*spaP$_{\Delta 666\text{-}Q252}$R^{251FLAG}S*	Made by Megaprimer from Plasmid pMIB5022. Megaprimer derived from pMIB7012 using SpaP45_seq_f + SpaQ_seq_r.
pMIB7043, SpaP$^{\text{^}S}$RS^{FLAG}	*spaP$_{\Delta 666\text{-}Q252}RS_{N258A}{}^{356FLAG}$*	Made by Megaprimer from Plasmid pMIB6089. Megaprimer derived from pMIB7012 using SpaP45_seq_f + SpaQ_seq_r.
pMIB7044, SpaQRP^{FLAG}S	*spaQRP^{84FLAG}S*	Made by Gibson assembly of PCR products of the following two primer/template pairs: 1. Insert: gib_spaQ_spaR_f + gib_spaS_spaP_r from pMIB7009; 2. Plasmid in two steps. Step1: SpaS_seq_f + SpaO_seq_r from pMIB7015 Step 2: gib_uni2_spaS_f + gib_uni_SpaQ_r from PCR product derived from Step 1
pMIB7045, SpaQR^{FLAG}PS	*spaQR^{251FLAG}PS*	Made by Gibson assembly of PCR products of the following two primer/template pairs: 1. Insert: gib_spaQ_spaR_f + gib_spaS_spaP_r from pMIB7008; 2. Plasmid in two steps. Step1: SpaS_seq_f + SpaO_seq_r from pMIB7015 Step 2: gib_uni2_spaS_f + gib_uni_SpaQ_r from PCR product derived from Step 1

pMIB7046, SpaQRPS^{FLAG}	*spaQRPS$_{N258A}$^{356FLAG}*	Made in two steps. 1. Plasmid used pMIB7045, Megaprimer derived from pMIB7010 using SpaR207_f and SpaO_seq_r. 2. Resulting plasmid from step 1 used with Megaprimer derived from pMIB7010 using gib_uni_SpaS272_f + prha_seq_r.
pMIB7047, SpaRQP^{FLAG}S	*spaRQP^{84FLAG}S*	Made in two steps. 1. Plasmid used pMIB7048, Megaprimer derived from pMIB7009 using SpaR207_f and SpaP_seq_r. 2. Resulting plasmid from step 1 used with Megaprimer derived from pMIB7010 using gib_uni_SpaS272_f + prha_seq_r.
pMIB7048, SpaQP$^{\wedge L}$R^{FLAG}S	*spaQPQ$_{\Delta 24\text{-}231}$R^{251FLAG}S*	Made by Gibson assembly of PCR products of the following two primer/template pairs: 1. Insert: gib_spaR_spaQ_f + gib_spaS_spaP_r from pMIB7017; 2. Plasmid: gib_uni2_spaS_f + gib_uni_spaR_r from pMIB7008
pMIB7049, SpaQP$^{\wedge L}$RS^{FLAG}	*spaQPQ$_{\Delta 24\text{-}231}$RS$_{N258A}$^{356FLAG}*	Made in two steps. 1. Plasmid used pMIB7048, Megaprimer derived from pMIB7009 using SpaR207_f and SpaP_seq_r. 2. Resulting plasmid from step 1 used with Megaprimer derived from pMIB7044 using gib_pT12_SpaP_f + SpaR_seq_r.

pMIB7050, SpaP^{FLAG}_QRS	*spaP^{84FLAG}$_{741+3}$::ins20QRS*	Made by Megaprimer from Plasmid pSB3704. Megaprimer derived from pMIB6670 using gib_SpaP164_f + SpaQ_seq_r2.
pMIB7051, SpaP_QR^{FLAG} S	*spaP$_{675+3}$QR^{251FLAG}S*	Made by Megaprimer from Plasmid pMIB5022. Megaprimer derived from pMIB6670 using gib_SpaP164_f + SpaQ_seq_r2.
pMIB7052, SpaP_QRS^{FLAG}	*spaP$_{675+3}$QRS$_{N258A}$^{356FLAG}*	Made by Megaprimer from Plasmid pMIB6089. Megaprimer derived from pMIB6670 using gib_SpaP164_f + SpaQ_seq_r2.
pMIB7053, SpaP^{FLAG}Q_RS	*spaP^{84FLAG}Q$_{261+1}$::ins20RS*	Made by Megaprimer from Plasmid pSB3704. Megaprimer derived from pMIB6610 using gib_SpaP164_f + SpaQ_seq_r2.
pMIB7054, SpaPQ_R^{FLAG}S	*spaPQ$_{261+1}$::ins20R^{251FLAG}S*	Made by Megaprimer from Plasmid pMIB5022. Megaprimer derived from pMIB6610 using gib_SpaP164_f + SpaQ_seq_r2.
pMIB7048, SpaQP^^{L}R^{FLAG}S	*spaQPQ$_{Δ24-231}$R^{251FLAG}S*	Made by Gibson assembly of PCR products of the following two primer/template pairs: 1. Insert: gib_spaR_spaQ_f + gib_spaS_spaP_r from pMIB7017; 2. Plasmid: gib_uni2_spaS_f + gib_uni_spaR_r from pMIB7008
pMIB7055, SpaPQ_RS^{FLAG}	*spaP$_{84}$^{FLAG}Q$_{261+1}$::ins20RS$_{N258A}$^{356FLAG}*	Made by Megaprimer from Plasmid pMIB6089. Megaprimer derived from pMIB6610 using gib_SpaP164_f + SpaQ_seq_r2.

pMIB7056, SpaP$^{FLAG\ \wedge L}$RQS	*spaP^{84FLAG}Q$_{\Delta 24-231}$RQS*	Made by Megaprimer from Plasmid pMIB7012. Megaprimer derived from pMIB7015 using gib_SpaP164_f + SpaQ_seq_r.
pMIB7057, SpaP$^{\wedge L}$R^{FLAG}QS	*spaPQ$_{\Delta 24-231}$R^{251FLAG}QS*	Made by Megaprimer from Plasmid pMIB7011. Megaprimer derived from pMIB7015 using gib_SpaP164_f + SpaQ_seq_r.
pMIB7058, SpaP$^{\wedge L}$RQS^{FLAG}	*spaPQ$_{\Delta 24-231}$RQS$_{N258A}$^{356FLAG}*	Made by Megaprimer from Plasmid pMIB7013. Megaprimer derived from pMIB7015 using gib_SpaP164_f + SpaQ_seq_r.
pMIB7059, SpaP^{FLAG}$_{A223KT224G}$QRS	*spaP^{84FLAG}$_{A223KT224G}$QRS*	Made by QuickChange from Plasmid SB3704. Primers used: SpaPA223KT224G_QC_f + SpaPA223KT224G_QC_r.
pMIB7127, SpaP$^{FLAG\ \wedge LM1K}$RQS	*spaP^{84FLAG}Q$_{2::a\Delta 24-231}$RQS*	PRQS mutated SpaQ remnant peptide inbetween *spaP* and *spaR*. Made by QC using Plasmid pMIB7056 and primer SpaQ_remnant_PR_M1K_QC_f + SpaQ_remnant_PR_M1K_QC_r
pMIB7128, SpaP $^{\wedge LM1K}$R^{FLAG}QS	*spaPQ$_{2::a\Delta 24-231}$R^{251FLAG}QS*	PRQS mutated SpaQ remnant peptide inbetween *spaP* and *spaR*. Made by QC using Plasmid pMIB7057 and primer SpaQ_remnant_PR_M1K_QC_f + SpaQ_remnant_PR_M1K_QC_r

pMIB7129, spaQP$^{FLAG\ \wedge LM1K}$RS	*spaQP^{84FLAG}Q$_{2::a\Delta 24\text{-}231}$RS*	QPRS mutated SpaQ remnant peptide inbetween *spaP* and *spaR*. Made by QC using Plasmid pMIB7015 and primer SpaQ_remnant_PR_M1K_QC_f + SpaQ_remnant_PR_M1K_QC_r
pMIB7130, spaQP$^{\wedge LM1K}$R^{FLAG}S	*spaQPQ$_{2::a\Delta 24\text{-}231}$R^{251FLAG}S*	QPRS mutated SpaQ remnant peptide inbetween *spaP* and *spaR*. Made by QC using Plasmid pMIB7016 and primer SpaQ_remnant_PR_M1K_QC_f + SpaQ_remnant_PR_M1K_QC_r

3 Results

In order to test the role of order of the *spaP, spaQ* and *spaR* genes in the assembly and function of the T3SS of *Salmonella enterica* serovar Typhimurium strain SL1344, I made the following modifications: For better handling, the flagella were removed and the fusion protein of the late effector SipA with nanoluciferase (SipA-NanoLuc) was chromosomally expressed to detect the secretion activity of late substrates of the T3SS. The *spaPQRS* operon was deleted from the chromosome to be able to selectively re-introduce the permutated genes into the bacteria on the low copy number plasmid pSB3398, resulting in the generation of strain MIB4592 (Table 6). To rule out possible influencing factors of the plasmid, strain MIB4592 was also complemented with control plasmids carrying the genes *spaP*, *spaQ* and *spaR* in the original order. Details on the plasmids carrying the genes in a permutated order are discussed below.

3.1 Selection of the constructs to be examined

Early work by Wagner *et al.*, revealed that a *spaS* null mutant can be episomally complemented (2010). Subsequently, Paroll could show that the gene order of the switch protein SpaS has no effect on the assembly and function of the export apparatus (2016). For this reason, I limited myself to the export apparatus genes *spaP*, *spaQ* and *spaR*, creating plasmids with all conceivable permutations (Table 8). Using as template chromosomal DNA of different *S.* Typhimurium SL1344 strains, lacking either *spaQ* or *spaR*, I rearranged and ligated individual genes using Gibson Assembly (see 2.3.1). For changes on shorter regions I used Megaprimer (see 2.3.3) and QuikChange site-directed mutagenesis (see 2.3.2). The low copy number plasmid pT10 (Figure 9 a) always served as backbone for the cloning of the genes in the new order. Insertion of the genes in the desired, *in silico* designed order was verified by sequencing.

For each permutation, I created three different variants each with a 3×FLAG tag on SpaP, SpaR, or SpaS, to allow immunodetection of the proteins (Figure 9 b). In this study, a mutant variant of SpaS with FLAG tag was used which cannot undergo autocleavage of SpaS in two subunits.

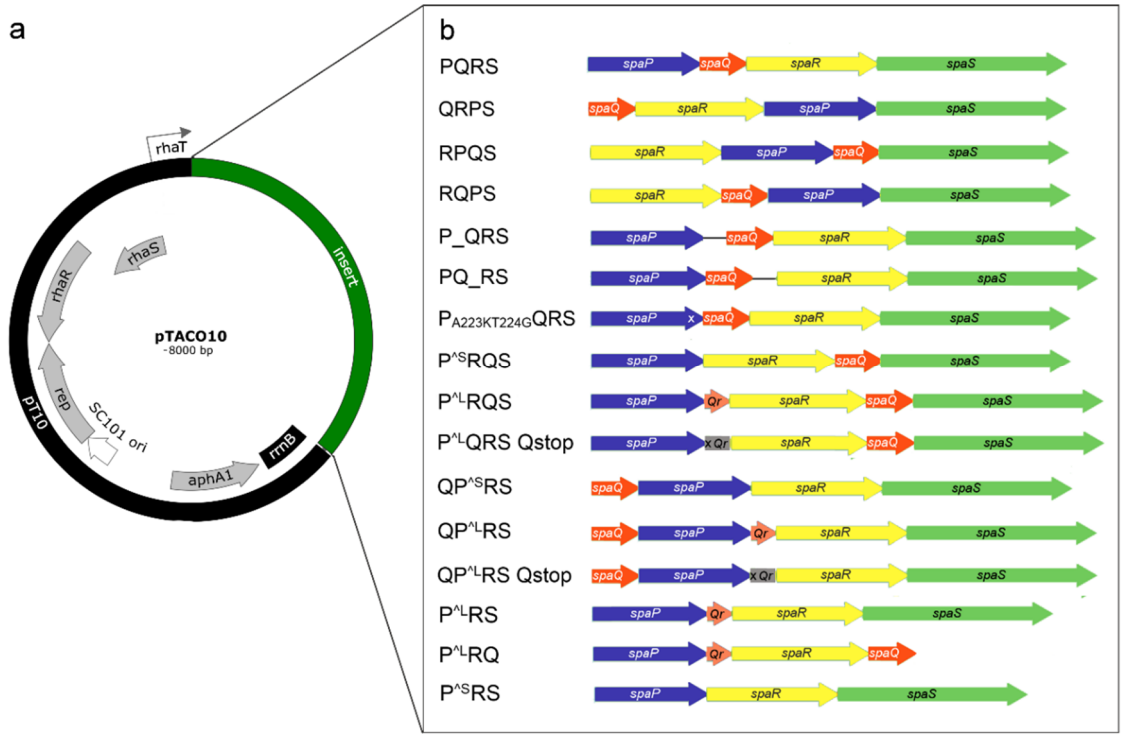

Figure 9: Plasmid pTACO10 and different constructs with alternated gene order (overview).
(a) Map of plasmid pTACO10. *aphA1*: Aminoglycoside 3'-phosphotransferase resistance gene for kanamycin; *rep*: ATP-dependent DNA helicase Rep; *rhaR* and *rhaS*: L-rhamnose responsive elements; *rhaT*: promoter; *rrnB*: terminator; *SC101ori*: origin of replication.
(b) Wild type PQRS and variations. x in $P_{A223KT224G}$QRS indicates the point mutation; *Qr*: SpaQ remnant peptide; x *Qr:* point mutation of the start codon of SpaQ remnant peptide.

A special feature I had to take into account was the transition between *spaQ* and *spaR*. The Shine-Dalgarno (SD) sequence of *spaR* overlaps with the coding sequence of *spaQ* in amino acid positions 85 and 86 (Figure 10 a). A conflict arose in the attempt to place *spaR* directly after *spaP* while retaining the original regulatory elements. On the one hand, I wanted to do justice to the translational coupling of *spaQ* and *spaR* and, on the other hand, I wanted to leave *spaP* unchanged (Figure 10 b). In order to take both aspects into account, I created two constructs with the same order but different approaches. In the case of P^LRQS (L stands for long), I left a fragment of *spaQ* between *spaP* and *spaR*,

but shortened it to 18 amino acids (Figure 10 c). Thus, *spaP* was unchanged and the SD of *spaR* was preserved as well, but a short, nonpolar SpaQ-remnant peptide was created. To investigate exclusively effects at the transcriptional level, I created another construct named $P^{\wedge LM1K}$RQS that has lysine (aag) instead of the start codon of the SpaQ remnant (Figure 10 e). The nucleotide sequence of $P^{\wedge LM1K}$RQS was identical to that of $P^{\wedge L}$RQS except for the mutation at the beginning, so to exclude confounding effects of the SpaQ remnant peptide.

To do justice to the spatial proximity of the two genes while leaving the SD sequence unchanged, I created another construct $P^{\wedge S}$RQS (S stands for short). To this aim, I changed the amino acids of SpaP in positions 245 and 246 from A and T to K and G, respectively (Figure 10 d). Thus, the artificial *spaP-spaR* transition resulted identical to the original *spaQ-spaR* transition. To investigate the pure, potentially distorting effect of the point mutation in *spaP* on complex assembly and function of T3SS, I created an additional construct by exchanging only two amino acids within SpaP in the context of an otherwise wild type operon ($P_{A245KT246G}$QRS).

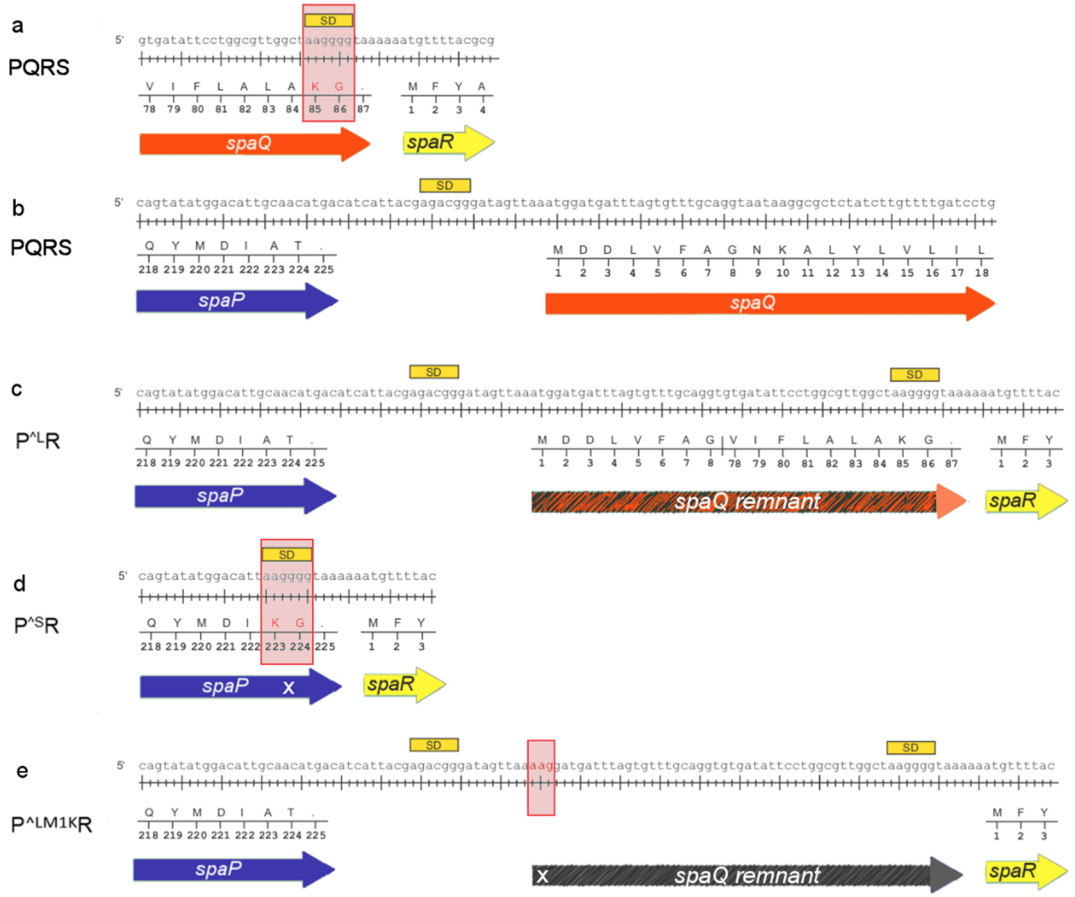

Figure 10: Overview of the different SD sequences and the *spaP-spaR* transitions of P^^{L}RQS and P^^{S}RQS.
(a) wild type: Transition from *spaQ* and *spaR* in detail, SD of *spaR* highlighted in red.
(b) wild type: Transition from *spaP* and *spaQ* in detail.
(c) P^^{L}R*:* Deletion of large parts of *spaQ*, with the SpaQ remnant consisting of the first 8 and the last 10 amino acids, here separated by a line. The SD sequence of *spaR* was preserved.
(d) P^^{S}R*:* Deletion of the SpaQ remnant and mutation of the amino acids in position 223 and 224 of *spaP* to keep the SD sequence identical. SD of *spaR* highlighted in red.
(e) P^^{LM1K}R*:* Point mutation of the start codon of SpaQ remnant to lysine (aag), marked in red.
SD: Shine-Dalgarno sequence.

To investigate the relevance of the spatial proximity of the *spaR* and *spaQ* genes, Zhou used a non-coding sequence of 20 nucleotides which was inserted between the two genes (Zhou 2017). These nucleotides are from now on referred to as "spacer". I used these spacers to create an artificial distance between *spaP* and *spaQ* and between *spaQ* and *spaR.* My intention was to test only the effect of a disconnection. As a result, the SD sequence and the distance to the downstream gene remained unchanged.

3.2 Creating the best starting conditions: Optimization of rhamnose induction

For this study, I used the L-rhamnose-inducible expression vector pT10, which was optimized for low copy number membrane protein expression (Wagner et al. 2008). Upon induction, bacterial cells need time to transcribe and translate the required proteins but, at the same time, rhamnose is metabolized by *S*. Typhimurium to a certain extent. This diminishes the amount of rhamnose available for induction. In order to find a balance between both effects and to obtain the maximum amount of proteins, I tested different time points of induction. While maintaining a total growth period of five hours, immediate induction and induction after one, two, three and four hours were tested (Figure 11 a). Secretion of SipA-NanoLuc was used as readout.

The SipA-NanoLuc-Assay (see 2.5) revealed a peak of secretion levels at two after induction. At three hours, the amount of secreted SipA-NanoLuc remained high, but diminished afterwards (Figure 11 b). To examine whether these dynamics in secretion were equally apparent in the amount of expressed proteins and the presence of the needle complex, I assessed expression of the core subunits and formation of the complex using SDS PAGE and BN PAGE, respectively. SDS PAGE (Figure 11 c) analysis revealed an increasing expression over time. Maximum expression was reached at the latest time point of induction. Complex formation as visualized with BN PAGE (Figure 11 d) showed a similar picture. The longer the time of induction, the more protein complexes became visible.

Taking both results into consideration, I decided for a time point of induction with rhamnose of three hours after the set-up of the back dilutions.

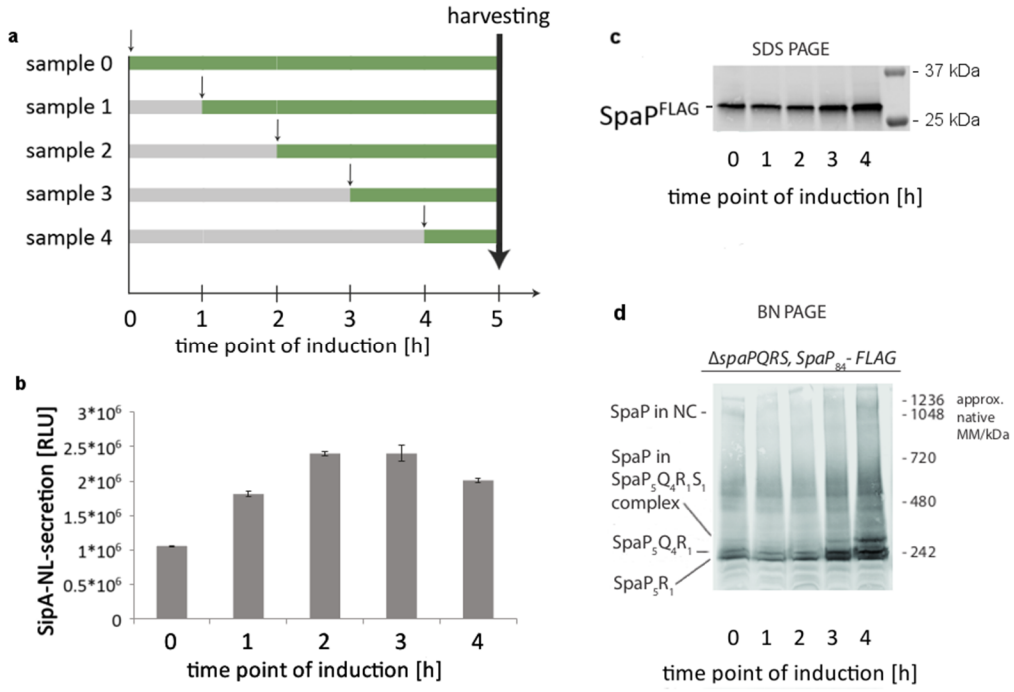

Figure 11: Optimization of rhamnose induction.
(a) Schematic view of the induction times. Small arrows: Time point of rhamnose induction, big arrow: Time point of harvesting after five hours of growth, green: Time of bacterial growth with rhamnose in medium.
(b) Secretion of SipA-NanoLuc of SpaP^{FLAG}QRS into the culture supernatant after different time points of rhamnose induction. RLU: relative luminescence units.
(c-d) Expression of membrane proteins (c) and analysis of complex assembly (d) after different time points of rhamnose induction, as detected with an anti–FLAG antibodies via SDS PAGE and Western Blot (c) or BN PAGE (d) of separated crude membranes of *Salmonella enterica* Typhimurium strain *ΔspaPQRS* complemented with pT10 plasmid carrying *spaPQRS* and *spaP^{84FLAG}*.

3.3 Changes in the gene sequence affect protein expression, complex formation and secretion activity

In order to examine the relevance of the gene order, I expressed the different constructs described above and analyzed protein expression by SDS PAGE, complex assembly by BN PAGE and overall function via the SipA-NanoLuc assay (Figure 12 and Figure 13).

With respect to SipA-NanoLuc secretion in the different backgrounds, all values are given relative to the luminescence measured for the *S.* Typhimurium strain SL1344 Δ*spaPQRS* complemented with plasmids carrying the original gene

order *spaPQRS (*referred to as *spaPQRS*$^{+}$*)* and expressing the tagged SpaP^{FLAG}, SpaR^{FLAG} or SpaS^{FLAG} variants, respectively.

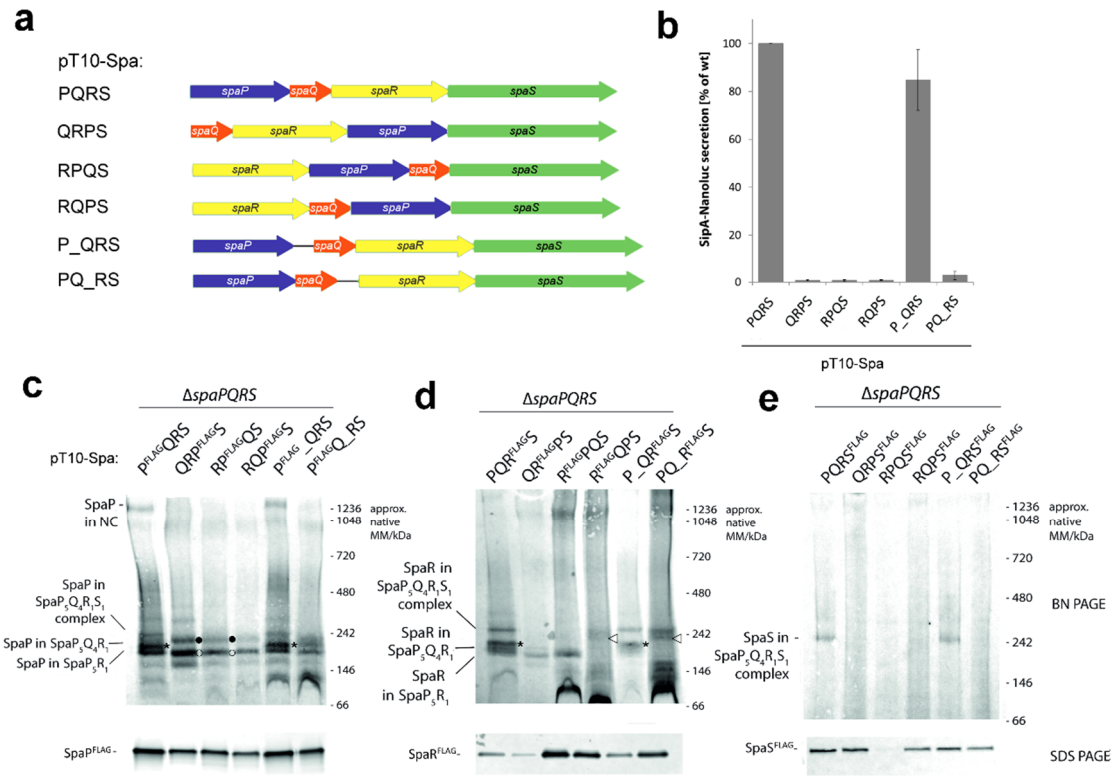

Figure 12: Comparison of the complex assembly and NanoLuc-luciferase signal as a measure of the secretion activity in strains carrying permutated *spaPQR* genes.
(a) Schematic overview of the constructs tested below. P_Q/Q_R: 20bp spacer inserted between two genes.
(b) NanoLuc-based secretion assay of different constructs carrying SpaP^{FLAG}. *spaPQRS*$^{+}$ set as 100%.
(c – e) Lauryl maltose neopentyl glycol (LMNG)-solubilized crude membranes obtained from *Salmonella enterica* Typhimurium strain MIB4592 (*ΔspaPQRS,* SipA-NL*, flhD::tet)* complemented with pTACO10 plasmids carrying (c) P^{FLAG}QRS, QRP^{FLAG}S, RP^{FLAG}QS, RQP^{FLAG}S, P^{FLAG}_QRS and P^{FLAG}Q_RS, (d) PQR^{FLAG}S, QR^{FLAG}PS, R^{FLAG}PQS, R^{FLAG}QPS, P_QR^{FLAG}S and PQ_R^{FLAG}S, (e) PQRS^{FLAG}, QRPS^{FLAG}, RPQS^{FLAG}, RQPS^{FLAG}, P_QRS^{FLAG} and PQ_RS^{FLAG}, were separated on BN PAGE and SDS PAGE and blotted with anti-FLAG antibodies. Constructs contain SpaP$_{84}$^{FLAG}, SpaR$_{251}$^{FLAG} or autocleavage-deficient SpaS$_{N258A356}$^{FLAG}. Shown is one out of three replicates. NC: needle complex, the triangle ◁ marks bands only appearing with SpaR^{FLAG}, the black dots ● mark bands only appearing in SpaP^{FLAG} the white dots ○ and the asterisk * mark bands that only appear in certain constructs, to allow better comparison among the different blots.

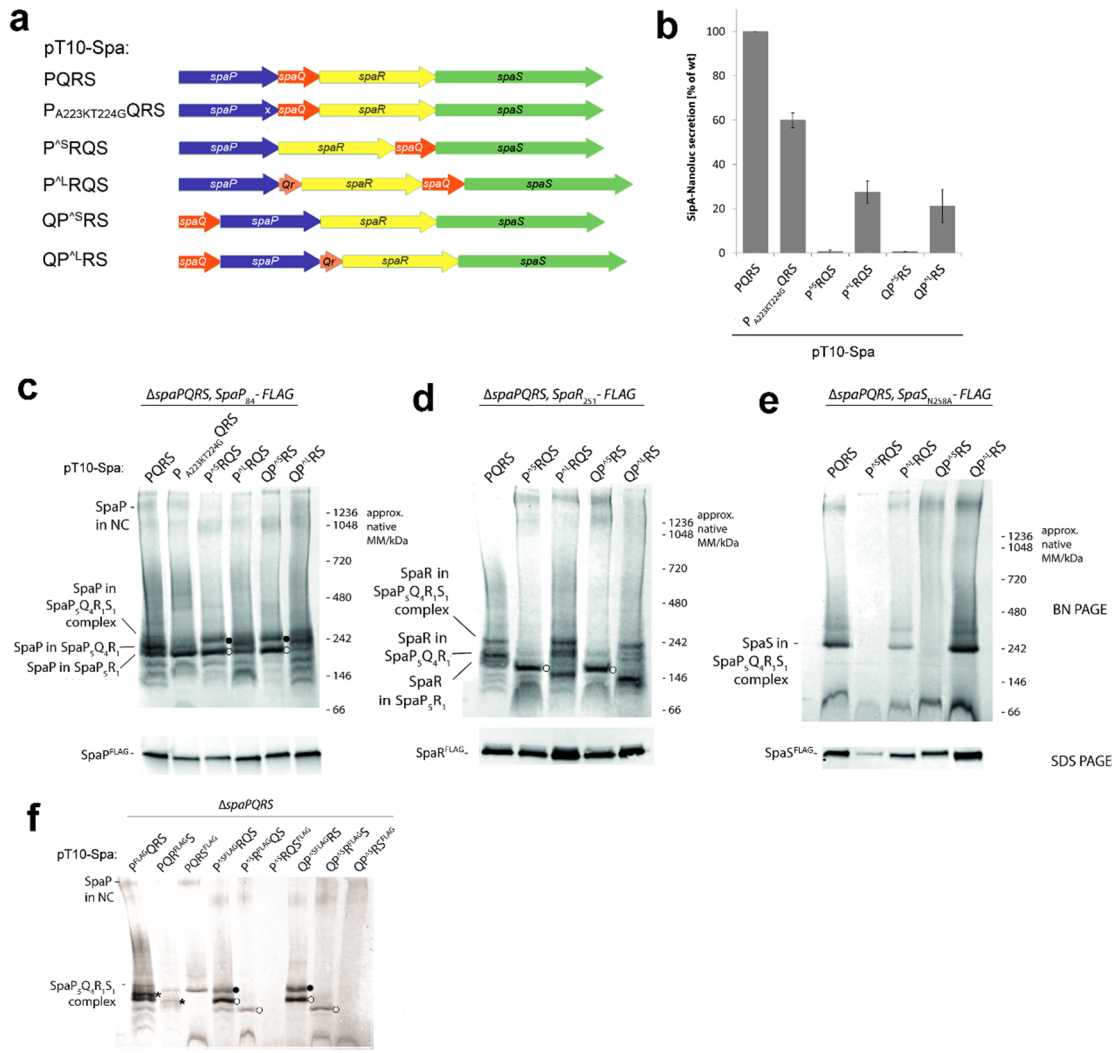

Figure 13: Comparison of the complex assembly and NanoLuc-luciferase signal as a measure of the secretion activity in strain carrying different *spaP-spaR* transitions.

(a) Schematic overview of the constructs tested. X indicates the point mutation *spaP*$_{A223KT224G}$, *Qr*:: SpaQ remnant.

(b) NanoLuc-based secretion assay of different constructs carrying SpaP^{FLAG}. *spaPQRS*$^{+}$ set as 100%. P$_{A245KT246G}$QRS: point mutation in *spaP*, P$^{\wedge S}$R: short version of the link between *spaP* and *spaR*, P$^{\wedge L}$R: long version of the link between *spaP* and *spaR* including SpaQ remnant peptide.

(c-f) LMNG-solubilized crude membranes obtained from *Salmonella enterica* Typhimurium strain MIB4592 (*ΔspaPQRS,* SipA-NL, *flhD::tet)* complemented with the following plasmids:

(c) PQRS, P$_{A223KT224G}$QRS, P$^{\wedge S}$RQS, P$^{\wedge L}$RQS, QP$^{\wedge S}$RS and QP$^{\wedge L}$RS (SpaP^{FLAG}).

(d) PQRS, P$^{\wedge S}$RQS, P$^{\wedge L}$RQS, QP$^{\wedge S}$RS and QP$^{\wedge L}$RS (SpaR^{FLAG}).

(e) PQRS, P$^{\wedge S}$RQS, P$^{\wedge L}$RQS, QP$^{\wedge S}$RS and QP$^{\wedge L}$RS (SpaS^{FLAG}), were separated on BN PAGE and SDS PAGE and blotted with anti-FLAG antibodies.

(f) Direct comparison of different FLAG tags of PQRS, P$^{\wedge S}$RQS and QP$^{\wedge S}$RS. Shown is one out of three replicates.

NC: needle complex, the asterisks * bands marked with ○ contain SpaP and SpaR, bands marked with ● contain SpaP but no other proteins.

The majority of the constructs (P^SRQS, QP^SRS, QRPS, RPQS, RQPS and PQ_RS) was unable to secrete SipA-NanoLuc, as indicated by secretion levels below 3%, compared to the wild type (Figure 12 b, Figure 13 b).
The sole point mutations in the 3' region of *spaP* (construct $P_{A245KT246G}QRS$) reduced the secretion to 60%, and still represented the third strongest secretion activity of all constructs.

The effect of disconnecting the two genes by introducing a 20 bp spacer while maintaining the original gene order depended on the location. Disconnecting *spaP* and *spaR* showed only a slight reduction of secretion efficiency to 90%, whereas disconnecting *spaR* and *spaQ* reduced the secretion to almost zero.

Interestingly, P^LRQS and QP^LRS (Figure 13 b) displayed low levels of secretion (27,6% and 21,3%).

The reduced secretion ability of strains carrying constructs with altered gene order raised the question to which extent and at which point the complex assembly was defective.

To test the hypothesis that a change in the gene order alters assembly as evidenced by a changed band pattern in the BN PAGE, I supplemented the *S*. Typhimurium strain MIB4592 (*ΔspaPQRS,* SipA-NL*, flhD::tet)* with plasmids carrying the following variants of the *spa* operon: PQRS (control), QRPS, RPQS, RQPS, P_QRS and PQ_RS (Figure 12 a). To be able to examine the composition of the formed complexes, each construct (including the controls) carried a tagged $SpaP^{FLAG}$ (Figure 12 c), $SpaR^{FLAG}$ (Figure 12 d) and $SpaS^{FLAG}$ variant (Figure 12 e), respectively.

The size of the solitary band at above 1200 kDa, that became visible with all three anti-FLAG antibodies (Figures 12 c, d, e and 13 c, d, e, f), indicated the presence of the needle complex as described by Wagner *et al.* (Wagner et al. 2010, p. 17745). The complex of SpaP, SpaQ, SpaR and SpaS was also visible with all three FLAG-tags at the same level of approximately 232 kDa (Figures 12 c, d, e and 13 c, d, e, f). The complexes of $P_5Q_4R_1$ and P_5R_1 could also be clearly

distinguished in the wildtype. The remaining bands were assembly intermediates, of which the composition cannot yet be determined.

With all three FLAG tags, the complex consisting of $SpaP_5Q_4R_1S_1$ was visible on the BN PAGE blot, particularly strong in PQRS and P_QRS (Figure 12 e). The band at about 220 kDa (marked with a black dot ●) just below the $SpaP_5Q_4R_1S_1$ complex with $SpaP^{FLAG}$ was better visible in the $P^{\wedge S}RQS$ and $QP^{\wedge S}RS$ constructs (Figure 13 c, d and f), but was also observable at the same height in RPQS and QRPS (Figure 12 c and d). There were no visible bands at the same height on the PAGE blots of the constructs with $SpaR^{FLAG}$ (Figure 12 d) or with $SpaS^{FLAG}$ (Figure 12 e), suggesting the sole presence of SpaP in the subcomplexes, possibly a complex constisting of 6 SpaP as described for $FliP_6$ in flagella.

In the same constructs a bit below at about 160 kDa, a band marked with a white dot (○) was visible with $SpaP^{FLAG}$ and particularly outstanding with $SpaR^{FLAG}$ possibly representing complexes with varying numbers of both proteins as $SpaP_4R_2$.

When *spaR* was located upstream of the other genes in the gene sequence or had no direct upstream gene due to the 20 bp spacer as in the case of RPQS, RQPS and PQ_RS, the expression of SpaR was increased, as shown by SDS PAGE (Figure 12 d, bottom panel).

In $RPQS^{FLAG}$, the expression of SpaS as visualized by SDS PAGE was extremely low in comparison to the other constructs. When comparing all three FLAG-tags, the band pattern of P_QRS was the most similar to that of PQRS. Especially with $SpaP^{FLAG}$ (Figure 12 c) and $SpaR^{FLAG}$ (Figure 12 d), the similarity of the bands marked with asterisk in both constructs was striking.

In the approach described in 3.1, two possible transition sequences between *spaP* and *spaR* were tested.

The constructs selected to observe possible effects of a changed transition between *spaP* and *spaR* were the following: PQRS (control), $P^{\wedge S}RQS$, $P^{\wedge L}RQS$, $QP^{\wedge S}RS$ and $QP^{\wedge L}RS$ (Figure 13 a). To be able to examine the composition of the

formed complexes, each construct carried a FLAG-tagged SpaP^{FLAG} (Figure 13 c), SpaR^{FLAG} (Figure 13 d) and SpaS^{FLAG} variant (Figure 13 e), respectively. In order to detect possible influences of the point mutation, P$^{FLAG}_{A223KT224G}$QRS was additionally examined in Figure 13 c.

When the connection between *spaP* and *spaR* was changed, the constructs P$^{\wedge S}$RQS and QP$^{\wedge S}$RS each stood out by band patterns that differed from PQRS, and visible in all three FLAG tags (Figure 13 c-e). Instead, P$^{\wedge L}$RQS showed similarities to QP$^{\wedge L}$RS, especially in SpaR^{FLAG} (Figure 13 d) and SpaS^{FLAG} (Figure 13 e). The band at the level of the expected SpaP$_5$Q$_4$R$_1$S$_1$ complex was clearly visible in both of these constructs. This was less apparent for P$^{FLAG}_{A223KT224G}$QRS. Nevertheless, bands similar to P^{FLAG}QRS were also visible here, although much more faded (Figure 13 c).

When looking at the construct QP$^{\wedge L}$RS, a larger amount of SpaS was noticeable in all replicates in both the BN PAGE and SDS PAGE blots (Figure 13 e).

To better compare the three FLAG tags, I loaded PQRS, P$^{\wedge S}$RQS and Q$^{\wedge S}$PRS side by side on a PAGE, alternating the FLAG tags (Figure 13 f).

The different running behavior of the FLAG tags must be taken into account. In Figure 13 f, an asterisk marks the same subcomplex containing SpaP and SpaR but running with different FLAGs at different heights. The same applies to the complexes marked with ○.

Comparing all three FLAG tags, it became clear that the uppermost band of the P$^{\wedge S}$R constructs (marked with a black dot ●) could not be the SpaP$_5$Q$_4$R$_1$S$_1$ complex, because it occurred exclusively in SpaP^{FLAG}.

There were differences between the isolated P-mutation and *spaPQRS*$^+$, but they were less pronounced when compared to the other constructs. Minor differences between P$^{\wedge L}$RQS and Q$^{\wedge L}$PRS were observable, as described above.

A change in the gene sequence resulted in bands of different height and intensity compared to the control. Differences in the presence and absence of the

$SpaP_5Q_4R_1S_1$ complex were particularly evident with $SpaR^{FLAG}$ and $SpaS^{FLAG}$. A separation of two genes using a 20 bp spacer while maintaining the original sequence showed almost no effect when located between *spaP* and *spaQ*, but when present between *spaQ* and *spaR* it led to the formation of complexes completely absent in the wild type.

When comparing the two *spaP-spaR* transitions, $P^{\wedge L}R$ looked more similar to the control than $P^{\wedge S}R$. This raised the question as to the reasons for the differences between the two versions.

3.4 Further investigation of the SpaQ remnant peptide

To investigate a possible influence of the SpaQ remnant peptide on the observed differences between $P^{\wedge L}R$ and $P^{\wedge S}R$, I created constructs with a point mutation in the SpaQ remnant gene to prevent translation ($P^{\wedge LM1K}RQS$ and $QP^{\wedge LM1K}RS$). I expressed the mutant SpaQ with either $SpaP^{FLAG}$ or $SpaR^{FLAG}$ and compared them with the controls PQRS and the two non-mutated constructs $P^{\wedge L}RQS$ and $QP^{\wedge L}RS$ (Figure 14 a).

The similarity of the band pattern of the non-mutated constructs in the BN PAGE to that of the control *spaPQRS*$^+$ was stronger when expressed with $SpaP^{FLAG}$ than with $SpaR^{FLAG}$ (Figure 14 c). With $SpaR^{FLAG}$, the $P^{\wedge L}RQS$ and $QP^{\wedge L}RS$ constructs showed a greater size dispersion of the bands (Figure 14 d). Nevertheless, in both cases the $SpaP_5Q_4R_1S_1$ complex was clearly visible in all BN PAGE blots. Interestingly, the band pattern of the point mutations resembles those of $P^{\wedge S}RQS$ and $QP^{\wedge S}RS$ (Figure 13).

When looking at the band intensity and the associated amount of protein in the SDS PAGE blot, a slight increase in the expression of SpaR in the two constructs $P^{\wedge L}RQS$ and $QP^{\wedge L}RS$ was noticeable for $SpaR_{251}^{FLAG}$ (Figure 14 d, bottom panel), and a decrease in the expression of SpaR in $P^{\wedge LM1K}RQS$ and $QP^{\wedge LM1K}RS$ when compared to PQRS.

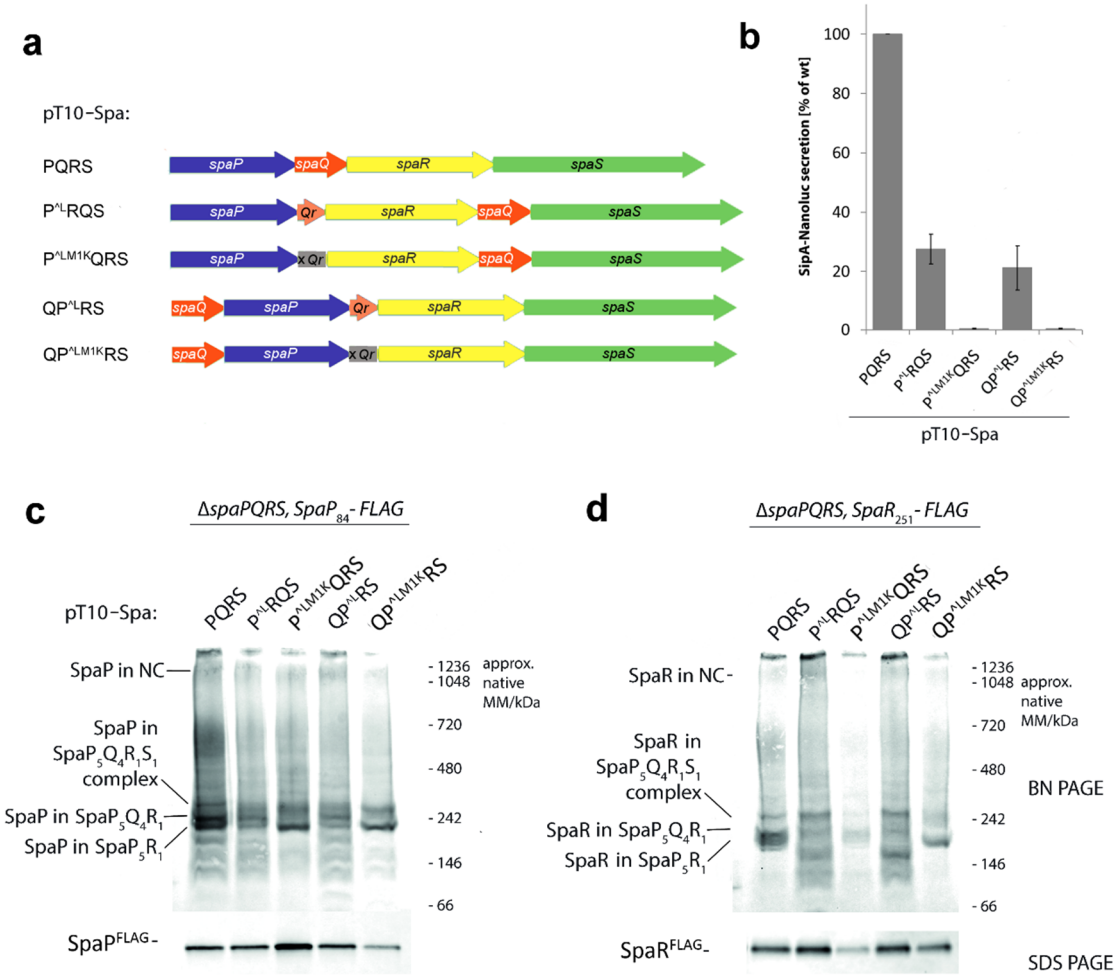

Figure 14: Effect of the SpaQ remnant peptide on complex assembly.
(a) Schematic overview of constructs tested below. *Qr*: SpaQ remnant. *x Qr:* SpaQ remnant with point mutation (*spaP^{M1K}R*) preventing translation.
(b) NanoLuc-based secretion assay of different constructs carrying SpaP^{FLAG}. *spaPQRS*$^{+}$ set as 100%.
(c – d) LMNG-solubilized crude membranes obtained from *S.* Typhimurium strain MIB4592 (*ΔspaPQRS,* SipA-NL, *flhD::tet)* complemented with the constructs (c) PQRS, P$^{\wedge L}$QRS, P$^{\wedge LM1K}$RQS, QP$^{\wedge L}$RS and QP$^{\wedge LM1K}$RS (SpaP^{FLAG}), and
(d) PQRS, P$^{\wedge L}$RQS, P$^{\wedge LM1K}$RQS, QP$^{\wedge L}$RS and QP$^{\wedge LM1K}$RS (SpaR^{FLAG}) were separated on BN PAGE and SDS PAGE and blotted with anti-FLAG antibodies. Shown is one out of three replicates. NC: needle complex

In both cases, a clearly altered pattern could be seen when the translation of the SpaQ remnant peptide was prevented by the point mutation. Since the position of *spaQ* seemed to have only little effect in both cases, we became interested to know which subcomplexes contain SpaQ.

3.5 Influence of *spaQ*

To unravel the role of SpaQ in the correct assembly of the core complex, we assessed in how many assembly intermediates SpaQ was present. To this aim, we compared constructs with deletion of either *spaQ* or *spaS* with constructs having either the longer *spaP-spaR* transition $P^{\wedge L}RQS$, which retained the SpaQ remnant peptide (Figure 15 b), or the shortened version $P^{\wedge S}RQS$ (Figure 15 c).

spaQ was deleted in the three constructs that carried a FLAG tag on a different complex component and compared on the same PAGE with control constructs still containing *spaQ.* Since the band patterns of PRQS and QPRS were similar (Figure 13 a-c), I limited myself to the order PRQS and did not additionally investigate QPRS. Both versions of the *spaP-spaR* transition were analyzed on a separate PAGE.

For the version containing the SpaQ remnant peptide (Figure 15 b), I used as control $P^{\wedge L}RQS$. To determine which bands are still present, I used the construct $P^{\wedge L}RS$, each tagged with $SpaP^{FLAG}$, $SpaR^{FLAG}$ and $SpaS^{FLAG}$, respectively. To observe the effect of a deletion of *spaS*, I added PRQ tagged with $SpaR^{FLAG}$.

For the shortened transition (Figure 15 c) I used as control $P^{\wedge S}RQS$. To visualize possible changes due to *spaQ* deletion, I used $P^{\wedge S}RS$. Each construct carried a FLAG-tagged $SpaP^{FLAG}$, $SpaR^{FLAG}$ and $SpaS^{FLAG}$ variant, respectively.

As expected, comparison of $P^{\wedge L}RQS^{FLAG}$ and $P^{\wedge L}RS^{FLAG}$ revealed a clear band at the level of the expected $SpaP_5Q_4R_1S_1$ complex in the presence, but not in the absence of *spaQ*. When comparing constructs $P^{\wedge L}RQS$ and $P^{\wedge L}RS$ as well as $P^{\wedge S}RQS$ and $P^{\wedge S}RS$, the strongest bands visible on both PAGE blots were present in both absence and presence of *spaQ*. Most likely, these represent subcomplexes containing SpaP and SpaR, but no SpaQ. With $P^{\wedge S}RQS$ and $P^{\wedge S}RS$ it became even more obvious that the bands visible in presence of *spaQ* were also apparent in its absence. $P^{\wedge L}RQS$ showed at least a couple of bands marked with a triangle ◄, which were not visible in the *ΔspaQ* version. With the exception of SpaS in the $SpaP_5Q_4R_1S_1$ complex, $SpaS^{FLAG}$ was not detectable,

not even in assembly intermediates. When *spaS* was missing, no $SpaP_5Q_4R_1S_1$ complex was detectable, just as in the absence of *spaQ*, and with $SpaR^{FLAG}$ (Figure 15 b) only a few, indistinct bands appeared on the PAGE blot.

Taken together, only a few of the bands were no longer visible when *spaQ* or *spaS* were deleted. After completion of the complex comparison, the functional assessment may provide further insights into the significance of the gene sequence.

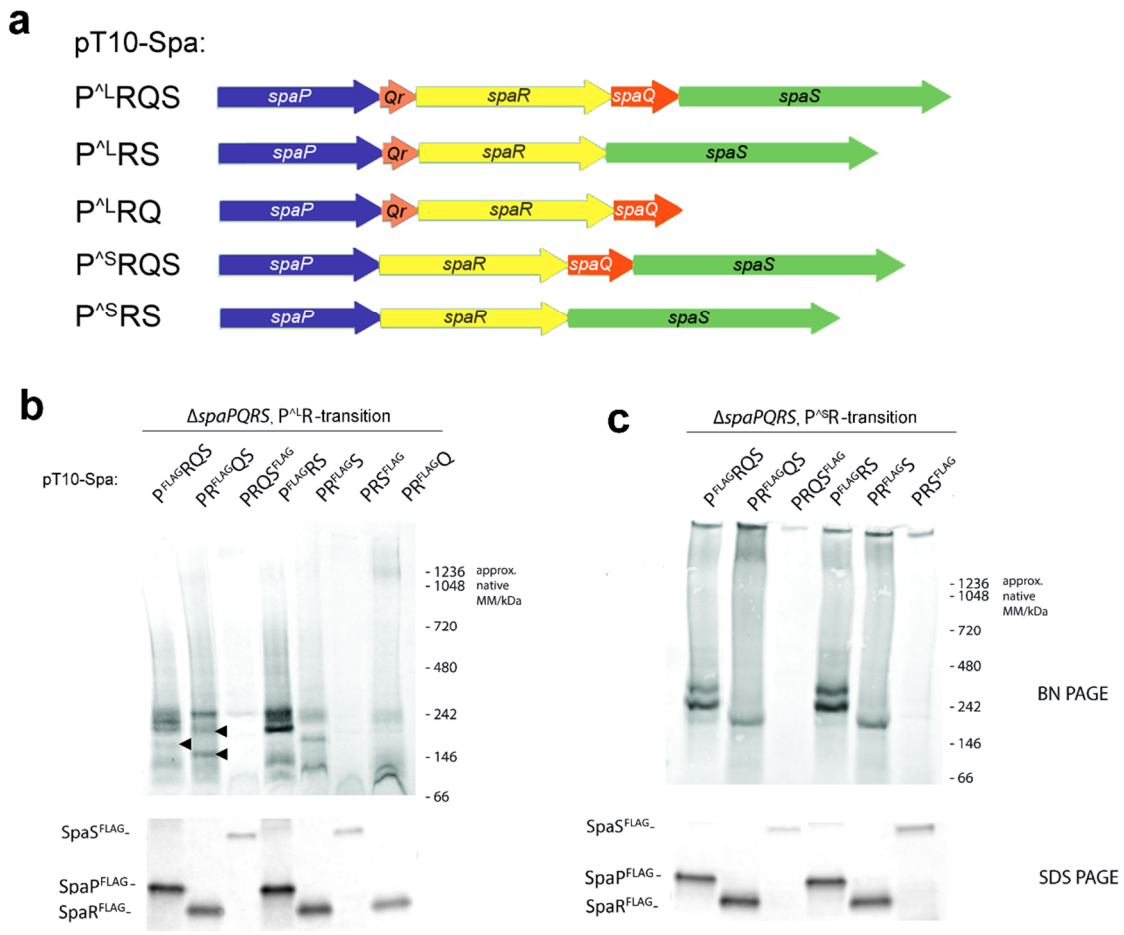

Figure 15: Direct comparison of constructs with and without *spaQ* or *spaS* with different FLAG-tagged components.
(a) Schematic overview of constructs tested below. *Qr*: SpaQ remnant.
(b-c) LMNG-solubilized crude membranes obtained from *Salmonella enterica* Typhimurium strain MIB4592 (*ΔspaPQRS,* SipA-NL*, flhD::tet)* complemented with the plasmids (b) long PR-transition ($P^{\wedge L}R$) of $P^{FLAG}RQS$, $PR^{FLAG}QS$, $PRQS^{FLAG}$, $P^{FLAG}RS$, $PR^{FLAG}S$, PRS^{FLAG} and $PR^{FLAG}Q$, and (c) short PR-transition ($P^{\wedge S}R$) of $P^{FLAG}RQS$, $PR^{FLAG}QS$, $PRQS^{FLAG}$, $P^{FLAG}RS$, $PR^{FLAG}S$ and PRS^{FLAG} were separated on BN PAGE and SDS PAGE and blotted with anti-FLAG antibodies. The position of the FLAG-tag is specified in the construct name Bands marked with a triangle ◄ are not visible in knockout versions. Shown is one out of three replicates.

4 Discussion

We know that the gene order of the components of the export apparatus is strongly conserved, in *Salmonella* as well as in *E*. *coli* and *Yersinia* (Hueck 1998). Conservation is often a sign of functional significance in evolution. This raises the questions: Does a change in the gene order have an influence on the assembly and function of the T3SS and if so, which one? Which conclusions can we draw from possible changes in the regulation and assembly of the export apparatus?

The aim of this work was to find out more about the regulation of the native genes encoding for the components of the T3SS. It thus represents an addition to the comprehensive work of Song *et al*., which dealt with gene scrambling, but in a rather artificial context. Indeed, they were placed under synthetic promoters, 5' untranslated regions, ribosome binding sites and terminators (Song et al. 2017). In contrast, my work focused more on the interaction and order of genes in the native context with the limitation of episomal expression.

When looking at the NanoLuc secretion (Figure 12 - Figure 14), it becomes clear that the vast majority of changes in the order of the genes leads to a strong reduction in the ability of secretion. This result supports the hypothesis that the original gene order is indispensable for the functionality of the complex and leads to the question which factors cause this drastic functional loss.

Any change in the gene sequence leads to a drastic reduction in secretion. In the case of the modified transition this is not exclusively due to the point mutation in SpaP, as shown in Figure 13. Direct comparison of the constructs helped in the search for explanations to the observed differences in secretion.

4.1 *spaQ* has a regulatory function in the assembly of the export apparatus

Differences in functionality and complex assembly of some constructs are related to the position of *spaQ*. If *spaQ* is upstream or downstream of *spaPR,* no effect is observed. However, *spaQ* in the transition between *spaP* and *spaR* seems to have a regulatory effect and prevents overexpression of *spaR*, which is consistent with the observations of Zhou (2017).

It was shown that the assembly order is 5 SpaP subunits and 1 SpaR subunit followed by 4 SpaQ subunits and finally 1 SpaS subunit (Wagner et al. 2010, Dietsche et al. 2016, Kuhlen et al. 2018, 2020). Considering the assembly order, the PRQS construct should actually work very efficiently. In a first attempt this assumption was not confirmed. And contrary to our expectations, the shortening of the transition from *spaP* to *spaR*, which was intended to lead to a more natural and thus more functional construct, had the opposite effect. It seems plausible that a more efficient assembly is due to the fact that SpaP and SpaR assemble together more efficiently when forming the initial complex.

A single mutation in the 3' region of *spaP* (construct $P_{A245KT246G}$QRS) in absence of any gene order change influences the band pattern representing the subcomplexes compared to *spaPQRS*$^{+}$ (Figure 13 c) without significantly affecting the secretion of SipA (Figure 13 b). This does not sufficiently explain the observed severe impairment of secretion in the constructs P$^{\wedge S}$RQS and QP$^{\wedge S}$RS to 0.8% and 0.7% (Figure 13 b), respectively, suggesting that factors other than the introduced point mutation influence functionality.

It is interesting that the constructs P$^{\wedge L}$RQS and QP$^{\wedge L}$RS apparently retain a residual functionality, which is, however, reduced by almost 80% compared to the wild type. The severe functional limitation is contrasted by an apparently effective complex assembly, also of the needle complex. This discrepancy cannot be explained by the BN PAGE. Possibly this is due to defective assembly despite correct stoichiometry e.g. due to incorrect SpaP-SpaR interaction. The comparison of the two constructs P$^{\wedge L}$R and P$^{\wedge S}$R shows that the presence or

absence of the SpaQ remnant peptide has a stronger impact on the assembly and function of the export apparatus than an influence on the mRNA structure. This could be shown with the insertion of a point mutation, which converted the start codon of the SpaQ remnant peptide to lysine and thus significantly reduced the secretion ability of the strain carrying this construct (Figure 14 b). The peptide upstream of *spaR* thus appears to have an important regulatory function, which is consistent with the observations of Paroll (2016). Interestingly, in terms of assembly and secretion levels the constructs $P^{\wedge S}RQS$ and $QP^{\wedge S}RS$ (Figure 13 c and d) show great similarity to $P^{\wedge LM1K}RQS$ and $QP^{\wedge LM1K}RS$ (Figure 14 c and d). In both cases, the common feature that no peptide is translated between *spaP* and *spaR* seems to play an important role.

The assembly of the $SpaP_5Q_4R_1S_1$ complex (see Figure 13 e) looks effective, but secretion is still reduced. Possibly the SpaQ remnant peptide binds somehow to SpaR, so that, on the one hand the $SpaR_x$ self-assembly is prevented. On the other hand, too strong binding reduces the secretion ability.

If the $SpaP_5R_1$ complex is defective, the assembly of SpaQ is less likely and, thus, also an addition of SpaS. Unassembled SpaQ and SpaS are probably degraded. Proteins that have been incorporated into the $SpaP_5Q_4R_1S_1$ complex at any time seem to be protected from degradation.

4.2 The wrong stoichiometry leads to self-assembly

The mRNA levels of the different genes within a polycistronic mRNA can be equal, even if the stoichiometry of the encoded proteins in the target complex is different. Here, the translational efficiency has a major influence and reflects the stoichiometry in the target complex (Li et al. 2014).

One possible explanation for the intermediate complex in QRPS, RPQS, RQPS and PQ_RS (marked with ● in Figure 12 c) would be a SpaP-only complex (Figure 16). Here, SpaP may not be able to interact with SpaR and aggregates with itself. For the SpaP homologue FliP in flagella from *Salmonella*, a $FliP_6$

complex was described by Fukumura *et al.* upon exclusive expression of *fliP* (2017). For unexplained reasons, the SpaP-only complex runs a little higher on the PAGE as described by Dietsche *et al*. (2016). Possibly the lower subcomplex (marked with ○ in Figure 12 c and Figure 13 c and d) consists of SpaP and SpaR, possibly in a dysfunctional stoichiometry, e.g. $SpaP_4R_2$ (Figure 16). However, the possibility of a stoichiometrically correct complex of $SpaP_5R_1$ cannot be excluded by the BN PAGE method alone.

Some of the assembly intermediates of the BN PAGEs might also contain different numbers of SpaQ (Figure 16). This effect of differential extraction with detergents was shown for Shigella flexneri, where complexes containing $SctR_5S_2T_1$ (corresponds to $SpaP_5Q_2R_1$ in S. Typhimurium), $SctR_5S_3T_1$ and $SctR_5S_4T_1$ were observed with cryo electron microscopy (Johnson et al. 2019).

As already reported (Dietsche et al. 2016), the assembly of SpaQ seems to be a critical factor. This could be confirmed in this study. Due to its small size, there is no functional FLAG- tagged version of SpaQ. To still be able to gain insight into the role of *spaQ*, I compared $P^{\wedge L}RQS$ and $P^{\wedge S}RQS$ with *spaQ* knockouts of the same construct (Figure 15 b and c). The comparison revealed the presence of the same subcomplexes independently of the presence of *spaQ* with few exceptions. These shared subcomplexes do not contain SpaQ. The subcomplexes marked with ◄ can be seen in $P^{\wedge L}RQS$, but are missing in the *spaQ* deletion mutant and could therefore contain *spaQ* (Figure 15 b). However, they do not appear in the PRQ construct. In the PAGE blots with $SpaS^{FLAG}$, SpaS is always only visible in the NC or $SpaP_5Q_4R_1S_1$ complex. Both together these data suggest that the extraction of the proteins with LMNG in combination with BN PAGE let SpaQ and SpaS appear only together in complexes. However, this seems to be related to the analytical technique used: in contrast to what observed here, Kuhlen *et al.* also report of complexes containing SpaQ without SpaS in their investigations of the export apparatus using mass spectrometry of membranes solubilized with LMNG (2018).

The subcomplexes visible in the constructs PQRS and P_QRS (marked with asterisk * in Figure 12 c and d, Figure 13 c, d and e) contain SpaP and SpaR.

SpaS is not part of this complex and no definite statement can be made about SpaQ. Considering the result that SpaQ only seems to be part of very few complexes (as described above, Figure 15 b), it is reasonable to assume that these bands probably consist of the initial $SpaP_5R_1$ complex, possibly with SpaQ.

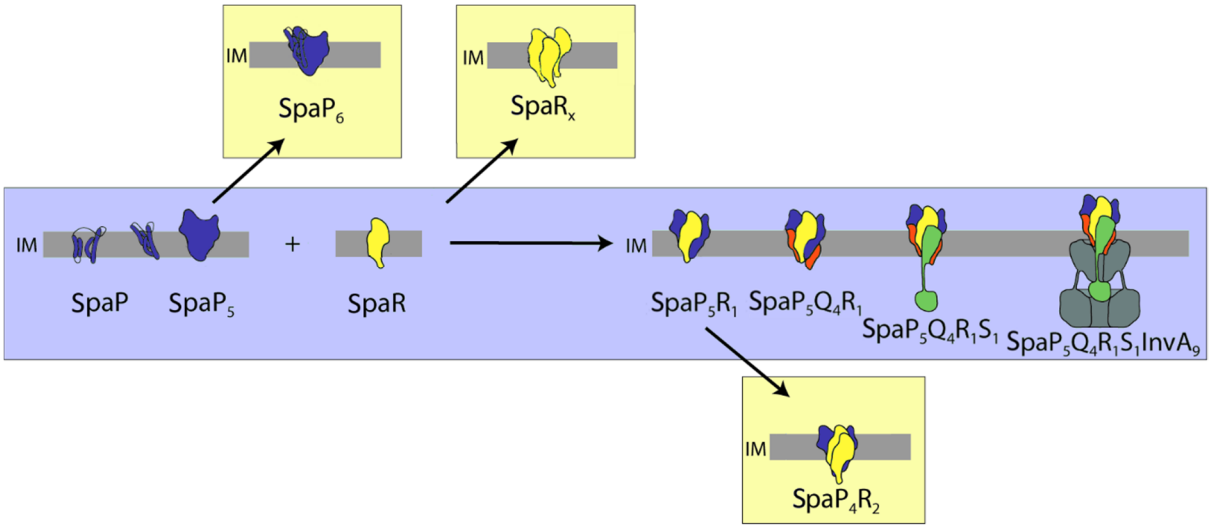

Figure 16: Possible defective assembly complexes of the export apparatus.
Correct assembly of the export apparatus (blue background), possible inefficient assembly complexes (yellow background), blue: SpaP, yellow: SpaR, orange: SpaQ, green: SpaS, grey: InvA
$SpaP_6$: Helical assembly as similarly observed in Flagella, $SpaR_x$: Suspected self-assembly of unknown SpaR quantity, $SpaP_4R_2$: Defective complex containing SpaP and SpaR in wrong stoichiometry, IM: Inner membrane

In the case of $R^{FLAG}PQS$, the significantly reduced amount of SpaS is striking. It does not seem plausible that SpaS would be particularly unstable here and therefore rapidly degraded. If the position of *spaQ* upstream of *spaS* were responsible for this, a reduced protein amount of SpaS would not only be observed in RPQS but also in $P^{\wedge L}RQS$ (Figure 12 e and Figure 13 e). The same effect cannot be observed if *spaQ* is upstream of *spaP*.

As shown by Zhou, due to the overlapping open reading frames of *spaR* and *spaQ*, a translational coupling of both proteins exists on the polycistronic mRNA (Zhou 2017). The disconnection of *spaQ* and *spaR* with a 20 bp spacer leads to the inability of complex assembly and secretion (Figure 12). It is possible that the ribosome cannot read continuously and detaches from the mRNA.

4.3 Overexpression of *spaR*

As similarly observed for the *spaQ* deletion mutant (Wagner et al. 2010), the accumulation levels of plasmid-expressed SpaR increased to above wild type levels in the absence of simultaneous coexpression of *spaP* and *spaQ* (Figure 12 c, bottom panel). Non-complexed proteins often end up in aggregates (Tyedmers et al. 2010). The excess of SpaR could statistically increase the probability of SpaR-only complex formation (Figure 16). SpaR might have the property of helical self-aggregation just like SpaP, since it is structurally similar to a fusion of SpaP and SpaQ (Kuhlen et al. 2018). The triangle ◁ indicates possible complexes that could represent such an assembly (Figure 12 d). This self-assemblies would make the attachment of further proteins impossible and thus represent a "dead end assembly".

Interestingly, overexpression of *spaR* does not affect *spaS*. The two genes overlap in *spaPQRS*$^{+}$ and the stoichiometry in the export apparatus is 1:1, so it is reasonable to assume that the two are regulatory coupled. This was neither confirmed when the transition between *spaR* and *spaS* was left unchanged (see P_QRS and PQ_RS in Figure 12 c and d) nor when the genes were separated (see RPQS in Figure 12 c and d).

Also in the SDS PAGE of the constructs P$^{\wedge L}$RQS and QP$^{\wedge L}$RS (Figure 13 d, bottom panel) the overexpression of SpaR is particularly noticeable. Despite an excess of SpaR, there is apparently no functionless self-assembly, as it might be the case with PQ_RS, RPQS and RQPS. One possible explanation could be that the proteins in the complex might be stabilized to such an extent that they are no longer degraded.

4.4 Technical limitations

The detergent LMNG is mild, which means that SpaQ and SpaS are still part of the complexes, and therefore allows distinguishing a large number of assembly complexes. The resulting intermediate complexes cannot be determined beyond doubt at this stage without further analysis, so that any interpretation of the

individual bands by comparison of the different PAGE blots has to be taken with caution.

To allow full comparison of the results of the NanoLuc assay with the PAGE analyses, I used the same constructs, i.e. those with the FLAG tag. With SpaS I would not have expected a secretion due to the autocleavage mutation. However, a secretion activity is actually detected. Although this is lower compared to $SpaP^{FLAG}$ and $SpaR^{FLAG}$, it shows the same signal differences in all the constructs carrying the different FLAG-tagged proteins (see Appendix).

The interpretation of the bands is further complicated by different running behavior in the PAGE. For instance, $SpaP^{FLAG}$ runs slightly higher on the PAGE than $SpaR^{FLAG}$ despite the lower molecular mass.

The fact that expression occurs from the plasmid and not from the genome could also have an influence.

4.5 Conclusion

Changes in the gene sequences have a massive impact on assembly and function of the T3SS. As soon as the original order *spaPQRS*$^{+}$ is changed, the secretion activity decreases to 0-30% compared to the wild type in all constructs. A decoupling of the genes in the original sequence using a 20 bp spacer shows only a minimal effect if inserted between *spaP* and *spaQ*. However, when inserted between *spaQ* and *spaR,* the spacer reduces the secretion activity below 3%.

Moreover, the individual permutations did lead to changes in complex assembly as shown by BN PAGE analysis. Especially five things are striking here. First: The less functional the construct is, the lower the expression of the $SpaP_5Q_4R_1S_1$ complex. Secondly, as soon as *spaR* is upstream of the other genes or has no gene directly upstream because of a spacer insertion, the expression of *spaR* is clearly increased. Thirdly, when *spaQ* is between *spaP* and *spaR*, it has a regulatory function and may take over the targeting of SpaR. To a limited extent,

this task might also be performed by the SpaQ remnant peptide, which has been shortened from 87 amino acids to 18 amino acids. Fourthly: Numerous assembly-intermediates are apparent. Possible explanations for individual bands could be self-aggregation of SpaR and a $SpaP_6$ aggregate as described for flagella in *Salmonella*. Fifthly, to a certain extent, the secondary structure of the mRNA can also have an influence, which is reflected in reduced expression of SpaS.

The newly acquired knowledge about gene regulation allows better understanding the export apparatus of T3SS of *S.* Typhimurium, and serves as basis for further studies to reduce bacterial pathogenicity

4.6 Outlook

Despite the attempts to make the linkage of the genes as natural as possible, it cannot be ruled out that the introduced changes have led to artificial errors that are not due to the genes but to other factors. To get as close as possible to the natural situation, a secretion assay with constructs that do not contain a FLAG tag would also be worth considering.

SpaS acts as internal control for the amount of protein analyzed because the band intensity on SDS-PAGE is mostly constant. SpaS is not affected by up- or downregulation, although it could be degraded. To ensure that the amount of mRNA is comparable, a control by real-time quantitative PCR would be necessary.

It would also be interesting to clarify whether the observed assembly defects arise during translation or during the assembly itself, i.e. whether less protein is produced from the outset or whether the proteins are degraded due to lack of complex formation. It is possible that a translational effect occurs, which would have to be investigated. A pulse chase assay can be used for this purpose.

In order to confirm with absolute certainty which proteins are present in the individual complexes visible as bands, further investigations are necessary. One possibility is immunoprecipitation followed by mass spectrometry.

Whether the unusual intermediate complexes are SpaR-SpaR aggregates could be investigated by *in vivo* photo-crosslinking. This involves the insertion of an unnatural amino acid *para*-benzoyl-L-phenylalanine (Bpa) at previously selected exposed positions. Under UV irradiation, Bpa forms a covalent bond with neighbouring amino acids, and these bonds are stable enough to be analyzed by other methods (Hino et al. 2005). This method could also be used to investigate whether the SpaQ remnant peptide present in P^LRQS and QP^LRS interacts with SpaR.

It would also be important to clarify whether the SpaQ remnant peptide itself carries out a function or the sole fact that something is translated between *spaP* and *spaR* impacts on the translation of these genes. This could be investigated, for instance by interposing GFP.

5 Summary

The T3SS is an important pathogenicity factor of *Salmonella enterica* Typhimurium. It is used to inject proteins directly into the host cell and enables the uptake of bacteria by intestinal cells. The correct assembly of a central component of the T3SS, the export apparatus, is crucial for the function of this molecular machine. The order of the genes encoding for the subunits of the export apparatus is highly conserved. In the present work, the effects of a changed order of the genes *spaP*, *spaQ* and *spaR* on the assembly and function of the T3SS were investigated. A *S*. Typhimurium Δ*spaPQRS* SipA-NL was used as background strain for the episomal expression of the *spaPQRS* operon with different permutations. Complex formation was investigated by BN PAGE analysis, and protein expression by SDS-PAGE analysis. Functionality of the system was estimated on the basis of effector secretion levels as quantified via the SipA-NanoLuc assay. The comparison of the different complexes revealed a significant reduction of the secretion ability of all constructs with altered gene order compared to *spaPQRS*$^{+}$. Among the most functional variants are those that show a SpaQ remnant peptide between *spaP* and *spaR*. Nonetheless, these do show a reduced secretion activity to 27.56% and 21.25%, respectively. Surprisingly, both the variants with a shortened *spaPR* transition without the SpaQ remnant peptide as well as those with a nonsense-mutation in the SpaQ remnant peptide have a drastically reduced secretion activity, i.e. below 1%. The most important finding of the work is the demonstration of the functional relevance of the conserved gene order. Furthermore, the data show that *spaQ* has a regulatory function that can be partially executed even when the gene is shortened to 54 base pairs. The role of SpaQ as well as the presence of possible defective intermediate complexes such as $SpaP_6$ and the $SpaR_x$-self-assemblies will require further investigation. Nevertheless, the work contributed to a better understanding of the assembly of the export apparatus and confirmed the importance of *spaQ* and the translational coupling of *spaQ* and *spaR*.

6 Deutsche Zusammenfassung

Das T3SS ist ein wichtiger Pathogenitätsfaktor von *Salmonella enterica* serovar Typhimurium. Es dient der Injektion von Proteinen direkt in die Wirtszelle und ermöglicht die Aufnahme von Bakterien in die Darmzellen. Der korrekte Zusammenbau einer zentralen Komponente des T3SS, des Exportapparats, ist entscheidend für die Funktion dieser molekularen Maschine. Die Reihenfolge der Gene, die für die Untereinheiten des Exportapparates kodieren, ist hoch konserviert. In der vorliegenden Arbeit wurden die Auswirkungen einer veränderten Anordnung der Gene *spaP*, *spaQ* und *spaR* auf den Aufbau und die Funktion der T3SS untersucht. S. Typhimurium *ΔspaPQRS* SipA-NL diente als Stamm für die episomale Expression des *spaPQRS*-Operons mit verschiedenen Permutationen. Die Komplexbildung wurde mittels BN-PAGE-Analyse und die Proteinexpression mittels SDS-PAGE-Analyse untersucht. Die Funktionalität des Systems wurde auf Basis der Effektorsekretionswerte geschätzt, die mittels SipA-NanoLuc-Assay quantifiziert wurden. Der Vergleich der verschiedenen Komplexe ergab eine signifikante Reduktion der Sekretionsfähigkeit aller Konstrukte mit veränderter Genreihenfolge im Vergleich zu *spaPQRS*$^{+}$. Zu den funktionellsten Varianten gehören diejenigen mit SpaQ-Restpeptid zwischen *spaP* und *spaR*. Nichtsdestotrotz zeigen diese eine reduzierte Sekretionsaktivität auf 27,56% bzw. 21,25%. Überraschenderweise haben sowohl die Varianten mit einem verkürzten *spaPR*-Übergang ohne das SpaQ-Restpeptid als auch die Varianten mit einer Nonsense-Mutation im SpaQ-Restpeptid eine drastisch reduzierte Sekretionsaktivität, d.h. unter 1%. Das wichtigste Ergebnis der Arbeit ist der Nachweis der funktionellen Relevanz der konservierten Genreihenfolge. Zudem zeigen die Daten, dass *spaQ* eine regulatorische Funktion hat, die teilweise auch ausgeführt werden kann, wenn das Gen auf 54 Basenpaare verkürzt ist. Die Rolle von SpaQ sowie das Vorhandensein möglicher defekter Intermediärkomplexe wie $SpaP_6$ und der $SpaR_x$ bedürfen weiterer Untersuchungen. Dennoch konnte die Arbeit einen Beitrag zum besseren Verständnis des Exportapparates leisten und die Bedeutung von *spaQ* und der translatorischen Kopplung von *spaQ* und *spaR* bestätigen.

7 Literature

Abby, S. S. and Rocha, E. P. C., 2012. The Non-Flagellar Type III Secretion System Evolved from the Bacterial Flagellum and Diversified into Host-Cell Adapted Systems. *PLoS Genetics*, 8 (9), e1002983.

Abrusci, P., Vergara-Irigaray, M., Johnson, S., Beeby, M. D., Hendrixson, D. R., Roversi, P., Friede, M. E., Deane, J. E., Jensen, G. J., Tang, C. M., and Lea, S. M., 2013. Architecture of the major component of the type III secretion system export apparatus. *Nature Structural & Molecular Biology*, 20 (1), 99–104.

Agilent, 2020. QuikChange II Site-Directed Mutagenesis Kit, Instruction Manual. [online]. Available from: https://www.agilent.com/cs/library/usermanuals/Public/200523.pdf. [Accessed 25 Feb 2020]

Bradley, 1994. Salmonella typhimurium initiates Murine Infection by Penetrating and Destroying the Specialized Epithelial M Cells of the Peyer's Patches. *The Journal of Experimental Medicine*, (Volume 180), 15–23.

Bundesinstitut für Risikobewertung, 2020. *Bedeutung der Salmonellen als Krankheitserreger* [online]. Available from: https://www.bfr.bund.de/de/bedeutung_der_salmonellen_als_krankheitserreger-537.html. [Accessed 26 Feb 2020]

Burkinshaw, B. J., Deng, W., Lameignère, E., Wasney, G. A., Zhu, H., Worrall, L. J., Finlay, B. B., and Strynadka, N. C. J., 2015. Structural Analysis of a Specialized Type III Secretion System Peptidoglycan-cleaving Enzyme. *Journal of Biological Chemistry*, 290 (16), 10406–10417.

Casali, N. and Preston, A., eds., 2003. *E. coli plasmid vectors: methods and applications*. Totowa, N.J: Humana Press.

Dandekar, T., 1998. Conservation of gene order: a fingerprint of proteins that physically interact. *Trends in Biochemical Sciences*, 23 (9), 324–328.

Diepold, A. and Wagner, S., 2014. Assembly of the bacterial type III secretion machinery. *FEMS Microbiology Reviews*, 38 (4), 802–822.

Dietsche, T., Tesfazgi Mebrhatu, M., Brunner, M. J., Abrusci, P., Yan, J., Franz-Wachtel, M., Schärfe, C., Zilkenat, S., Grin, I., Galán, J. E., Kohlbacher, O., Lea, S., Macek, B., Marlovits, T. C., Robinson, C. V., and Wagner, S., 2016. Structural and Functional Characterization of the Bacterial Type III Secretion Export Apparatus. *PLOS Pathogens*, 12 (12), e1006071.

Eitinger, T., 2017. *Allgemeine Mikrobiologie*. 10., unveränderte Auflage. Stuttgart New York: Georg Thieme Verlag.

Fabiani, F. D., Renault, T. T., Peters, B., Dietsche, T., Gálvez, E. J. C., Guse, A., Freier, K., Charpentier, E., Strowig, T., Franz-Wachtel, M., Macek, B., Wagner, S., Hensel, M., and Erhardt, M., 2017. A flagellum-specific chaperone facilitates assembly of the core type III export apparatus of the bacterial flagellum. *PLOS Biology*, 15 (8), e2002267.

Figueira, R. and Holden, D. W., 2012. Functions of the Salmonella pathogenicity island 2 (SPI-2) type III secretion system effectors. *Microbiology*, 158 (5), 1147–1161.

Fukumura, T., Makino, F., Dietsche, T., Kinoshita, M., Kato, T., Wagner, S., Namba, K., Imada, K., and Minamino, T., 2017. Assembly and stoichiometry of the core structure of the bacterial flagellar type III export gate complex. *PLOS Biology*, 15 (8), e2002281.

Gibson, A. M., Bratchell, N., and Roberts, T. A., 1988. Predicting microbial growth: growth responses of salmonellae in a laboratory medium as affected by pH, sodium chloride and storage temperature. *International Journal of Food Microbiology*, 6 (2), 155–178.

Gibson, D. G., Young, L., Chuang, R.-Y., Venter, J. C., Hutchison, C. A., and Smith, H. O., 2009. Enzymatic assembly of DNA molecules up to several hundred kilobases. *Nature Methods*, 6 (5), 343–345.

Goessweiner-Mohr, N., Kotov, V., Brunner, M. J., Mayr, J., Wald, J., Kuhlen, L., Miletic, S., Vesper, O., Lugmayr, W., Wagner, S., DiMaio, F., Lea, S., and Marlovits, T. C., 2019. *Structural control for the coordinated assembly into functional pathogenic type-3 secretion systems* [online]. Molecular Biology. preprint. Available from: http://biorxiv.org/lookup/doi/10.1101/714097 [Accessed 6 Oct 2019].

Gophna, U., Ron, E. Z., and Graur, D., 2003. Bacterial type III secretion systems are ancient and evolved by multiple horizontal-transfer events. *Gene*, 312, 151–163.

Hansen-Wester, I. and Hensel, M., 2001. Salmonella pathogenicity islands encoding type III secretion systems. *Microbes and Infection*, 3 (7), 549–559.

Haraga, A., Ohlson, M. B., and Miller, S. I., 2008. Salmonellae interplay with host cells. *Nature Reviews Microbiology*, 6 (1), 53–66.

Hardie, K. R., Lory, S., and Pugsley, A. P., 1996. Insertion of an outer membrane protein in Escherichia coli requires a chaperone-like protein. *The EMBO Journal*, 15 (5), 978–988.

Hino, N., Okazaki, Y., Kobayashi, T., Hayashi, A., Sakamoto, K., and Yokoyama, S., 2005. Protein photo-cross-linking in mammalian cells by site-specific incorporation of a photoreactive amino acid. *Nature Methods*, 2 (3), 201–206.

Hueck, C. J., 1998. Type III Protein Secretion Systems in Bacterial Pathogens of Animals and Plants. *Microbiology and Molecular Biology Reviews*, 62 (2), 379–433.

John E.G. McCarthy and Claudio Gualerzi, 1990. Translational control of prokaryotic gene expression. *Elsevier Science Publishers Ltd. (UK)*, 6 (3), 78–85.

Johnson, S., Kuhlen, L., Deme, J. C., Abrusci, P., and Lea, S. M., 2019. gop. *mBio*, 10 (3), 50.

Kuhlen, L., Abrusci, P., Johnson, S., Gault, J., Deme, J., Caesar, J., Dietsche, T., Mebrhatu, M. T., Ganief, T., Macek, B., Wagner, S., Robinson, C. V., and Lea, S. M., 2018. *Structure of the Core of the Type Three Secretion System Export Apparatus* [online]. Microbiology. preprint. Available from: http://biorxiv.org/lookup/doi/10.1101/249128 [Accessed 26 Feb 2020].

Kuhlen, L., Johnson, S., Zeitler, A., Bäurle, S., Deme, J. C., Caesar, J. J. E., Debo, R., Fisher, J., Wagner, S., and Lea, S. M., 2020. The substrate

specificity switch FlhB assembles onto the export gate to regulate type three secretion. *Nature Communications*, 11 (1), 1296.
Kyte, J. and Doolittle, R. F., 1982. A simple method for displaying the hydropathic character of a protein. *Journal of Molecular Biology*, 157 (1), 105–132.
Laemmli, U. K., 1970. Cleavage of Structural Proteins during the Assembly of the Head of Bacteriophage T4. *Nature*, 227 (5259), 680–685.
Lara-Tejero, M., Kato, J., Wagner, S., Liu, X., and Galan, J. E., 2011. A Sorting Platform Determines the Order of Protein Secretion in Bacterial Type III Systems. *Science*, 331 (6021), 1188–1191.
Lavander, M., Sundberg, L., Edqvist, P. J., Lloyd, S. A., Wolf-Watz, H., and Forsberg, A., 2002. Proteolytic Cleavage of the FlhB Homologue YscU of Yersinia pseudotuberculosis Is Essential for Bacterial Survival but Not for Type III Secretion. *Journal of Bacteriology*, 184 (16), 4500–4509.
Lerminiaux, N. A., MacKenzie, K. D., and Cameron, A. D. S., 2020. Salmonella Pathogenicity Island 1 (SPI-1): The Evolution and Stabilization of a Core Genomic Type Three Secretion System. *Microorganisms*, 8 (4), 576.
Li, G.-W., 2015. How do bacteria tune translation efficiency? *Current Opinion in Microbiology*, 24, 66–71.
Li, G.-W., Burkhardt, D., Gross, C., and Weissman, J. S., 2014. Quantifying Absolute Protein Synthesis Rates Reveals Principles Underlying Allocation of Cellular Resources. *Cell*, 157 (3), 624–635.
Macnab, R. M., 2004. Type III flagellar protein export and flagellar assembly. *Biochimica et Biophysica Acta (BBA) - Molecular Cell Research*, 1694 (1–3), 207–217.
Majowicz, S. E., Musto, J., Scallan, E., Angulo, F. J., Kirk, M., O'Brien, S. J., Jones, T. F., Fazil, A., and Hoekstra, R. M., 2010. The Global Burden of Nontyphoidal *Salmonella* Gastroenteritis. *Clinical Infectious Diseases*, 50 (6), 882–889.
Marlovits, T. C., Kubori, T., Lara-Tejero, M., Thomas, D., Unger, V. M., and Galan, J. E., 2006. Assembly of the inner rod determines needle length in the type III secretion injectisome, 441, 4.
Monjarás Feria, J. V., Lefebre, M. D., Stierhof, Y.-D., Galán, J. E., and Wagner, S., 2015. Role of Autocleavage in the Function of a Type III Secretion Specificity Switch Protein in *Salmonella enterica* Serovar Typhimurium. *mBio*, 6 (5), e01459-15.
Mueller, C. A., Broz, P., and Cornelis, G. R., 2008. The type III secretion system tip complex and translocon. *Molecular Microbiology*, 68 (5), 1085–1095.
Naum, M., Brown, E. W., and Mason-Gamer, R. J., 2009. Phylogenetic evidence for extensive horizontal gene transfer of type III secretion system genes among enterobacterial plant pathogens. *Microbiology*, 155 (10), 3187–3199.
New England Biolabs, 2020a. *High Efficiency Transformation Protocol* [online]. Available from: https://international.neb.com/protocols/0001/01/01/high-efficiency-transformation-protocol-c2987. [Accessed 26 Feb 2020]
New England Biolabs, 2020b. *NEB® 5-alpha Competent E. coli* [online]. Available from: https://international.neb.com/products/c2988-neb-5-alpha-competent-e-coli-subcloning-efficiency#Product%20Information.

Paroll, C., 2016. Assembly quality control and turn-over of export apparatus components of bacterial type III secretion systems. Master's thesis. Eberhard-Karls Universität, Tübingen.

Robert-Koch Institut, 2019. Infektionsepidemiologisches Jahrbuch meldepflichtiger Krankheiten für 2018. [online]. Available from: https://www.rki.de/DE/Content/Infekt/Jahrbuch/Jahrbuch_2018.pdf?__blob=publicationFile. [Accessed 26 Feb 2020]

Schägger, H. and von Jagow, G., 1991. Blue native electrophoresis for isolation of membrane protein complexes in enzymatically active form. *Analytical Biochemistry*, 199 (2), 223–231.

Song, M., Sukovich, D. J., Ciccarelli, L., Mayr, J., Fernandez-Rodriguez, J., Mirsky, E. A., Tucker, A. C., Gordon, D. B., Marlovits, T. C., and Voigt, C. A., 2017. Control of type III protein secretion using a minimal genetic system. *Nature Communications*, 8, 14737.

Sukhan, A., Kubori, T., Wilson, J., and Galán, J. E., 2001. Genetic Analysis of Assembly of theSalmonella enterica Serovar Typhimurium Type III Secretion-Associated Needle Complex. *Journal of Bacteriology*, 183 (4), 1159–1167.

Tyedmers, J., Mogk, A., and Bukau, B., 2010. Cellular strategies for controlling protein aggregation. *Nature Reviews Molecular Cell Biology*, 11 (11), 777–788.

Wagner, S., Grin, I., Malmsheimer, S., Singh, N., Torres-Vargas, C. E., and Westerhausen, S., 2018. Bacterial type III secretion systems: a complex device for the delivery of bacterial effector proteins into eukaryotic host cells. *FEMS Microbiology Letters* [online], 365 (19). Available from: https://academic.oup.com/femsle/article/doi/10.1093/femsle/fny201/5068689 [Accessed 2 Apr 2020].

Wagner, S., Klepsch, M. M., Schlegel, S., Appel, A., Draheim, R., Tarry, M., Hogbom, M., van Wijk, K. J., Slotboom, D. J., Persson, J. O., and de Gier, J.-W., 2008. Tuning Escherichia coli for membrane protein overexpression. *Proceedings of the National Academy of Sciences*, 105 (38), 14371–14376.

Wagner, S., Königsmaier, L., Lara-Tejero, M., Lefebre, M., Marlovits, T. C., and Galán, J. E., 2010. Organization and coordinated assembly of the type III secretion export apparatus. *Proceedings of the National Academy of Sciences*, 107 (41), 17745–17750.

Westerhausen, S., Nowak, M., Torres-Vargas, C., Bilitewski, U., Bohn, E., Grin, I., and Wagner, S., 2019. *A NanoLuc luciferase-based assay enabling the real-time analysis of protein secretion and injection by bacterial type III secretion systems* [online]. Microbiology. preprint. Available from: http://biorxiv.org/lookup/doi/10.1101/745471 [Accessed 6 Oct 2019].

White, S. H. and von Heijne, G., 2004. The machinery of membrane protein assembly. *Current Opinion in Structural Biology*, 14 (4), 397–404.

World Health Organization, 2020. *Fact Sheet Salmonella (non-typhoidal)* [online]. Available from: https://www.who.int/en/news-room/fact-sheets/detail/salmonella-(non-typhoidal).

Zhou, D., 1999. Role of the S. Typhimurium Actin-Binding Protein SipA in Bacterial Internalization. *Science*, 283 (5410), 2092–2095.

Zhou, J., 2017. Translational Coupling of the Type III secretion system (T3SS) genes spaQ and spaR in Salmonella. Master's thesis. Eberhard-Karls Universität, Tübingen.

Zilkenat, S., Franz-Wachtel, M., Stierhof, Y.-D., Galán, J. E., Macek, B., and Wagner, S., 2016. Determination of the Stoichiometry of the Complete Bacterial Type III Secretion Needle Complex Using a Combined Quantitative Proteomic Approach. *Molecular & Cellular Proteomics*, 15 (5), 1598–1609.

8 Appendix

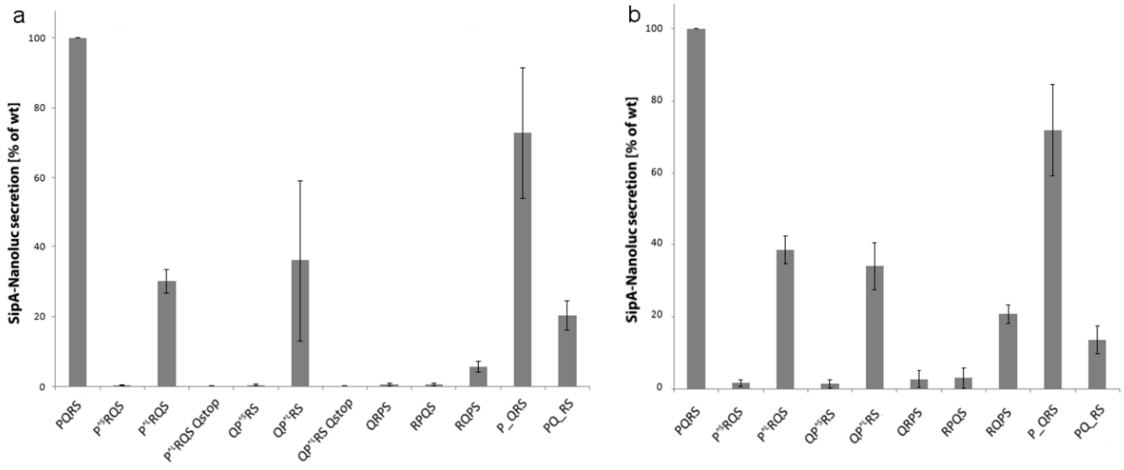

Figure 17: NanoLuc-luciferase signal as a measure of the secretion activity from different constructs in percentage of the wild type *spaPQRS*$^{+}$.
NanoLuc-based secretion assay of *spaPQRS*$^{+}$ set as 100%.
(a) Constructs with R^{FLAG}. P$^{\wedge S}$R: short version of the link between *spaP* and *spaR*, P$^{\wedge L}$R: long version of the link between *spaP* and *spaR* including SpaQ remnant peptide, P$^{\wedge LM1K}$R: P$^{\wedge L}$R with point mutation of the start codon of SpaQ remnant, preventing the peptide to be made, P_Q/Q_R: 20bp spacer inserted between two genes.
(b) Constructs with S^{FLAG}.

Table 9: Relative secretion activity compared to the wild type in constructs containing SpaP^{FLAG}.

Plasmid (pMIB) number	Name	relative secretion activity (wt 100%)
3704	PQRS	100
7059	P$_{A223KT224G}$QRS	59.93
7012	P$^{\wedge S}$RQS	0.79
7056	P$^{\wedge L}$RQS	27.56
7127	P$^{\wedge LM1K}$RQS	0.35
7018	QP$^{\wedge S}$RS	0.67
7015	QP$^{\wedge L}$RS	21.25
7129	QP$^{\wedge LM1K}$RS	0.34
7044	QRPS	0.69
7009	RPQS	0.73
7047	RQPS	0.82
7050	P_QRS	84.72
7053	PQ_RS	2.79

9 Erklärung zum Eigenanteil

Die Arbeit wurde im Interfakultären Institut für Mikrobiologie und Infektionsmedizin unter Betreuung von Prof. Samuel Wagner und Mentorat von Dr. Iwan Grin durchgeführt.
Die Konzeption der Studie erfolgte durch Samuel Wagner, Professor für Infektionsbiologie.

Sämtliche Versuche wurden nach Einarbeitung durch Labormitglieder Andrea Eipper, Dr. Iwan Grin, Nidhi Singh und Sibel Westerhausen von mir eigenständig durchgeführt.

Ich versichere, das Manuskript selbständig verfasst zu haben und keine weiteren als die von mir angegebenen Quellen verwendet zu haben. Anmerkungen zum Manuskript erfolgten durch Prof. Samuel Wagner, Dr. Iwan Grin und Dr. Libera Lo Presti.

Sämtliche Grafiken, wenn nicht anders vermerkt, habe ich selbst erstellt.

Im Nachgang der hier beschriebenen Arbeiten stellte sich heraus, dass einige der von mir generierten Plasmide eine Punktmutation in SpaP (S178R) enthielten, die ich nicht zu verschulden habe. Folgende Plasmide sind davon betroffen:

Plasmid (pMIB) Nummer	Name	betroffene Abbildung
7044	QRP^{FLAG}S	12
7045	QR^{FLAG}PS	
7046	QRPS^{FLAG}	
7009	RP^{FLAG}QS	
7008	R^{FLAG}PQS	
7010	RPQS^{FLAG}	

Plasmid (pMIB) Nummer	Name	betroffene Abbildungen
7012	P$^{FLAG\wedge S}$RQS	13, 15
7011	P$^{\wedge S}$R^{FLAG}QS	
7013	P$^{\wedge S}$RQS^{FLAG}	
7018	QP$^{FLAG\wedge S}$RS	13
7019	QP$^{\wedge S}$R^{FLAG}S	
7020	QP$^{\wedge S}$RS^{FLAG}	
7041	P$^{FLAG\wedge S}$RS	15
7042	P$^{\wedge S}$R^{FLAG}S	
7043	P$^{\wedge S}$RS^{FLAG}	

Diese Mutation führt zu einem Assemblierungsdefekt von SpaP, so dass die Assemblierungs- und Stabilitätsdaten der von der Mutation betroffenen Konstrukte hinfällig sind. Nacharbeiten haben allerdings ergeben, dass die grundsätzliche Aussage, dass die Reihenfolge der Gene des Exportapparats für die Effizienz der Assemblierung zwingend ist, weiterhin Bestand hat.

Tübingen, den

Mirjam Forberger

10 Danksagung

Auf der Titelseite steht nur ein Name, tatsächlich aber haben mich viele Menschen auf unterschiedlichste Weise unterstützt und dafür möchte ich aus ganzem Herzen Danke sagen.

Zuallererst möchte ich dir, Samuel, herzlich danken. Der Zuteilungsalgorithmus der Fakultät mag in meinem ersten Semester dafür gesorgt haben, dass sich unsere Wege kreuzten. Dass ich seitdem den Salmonellen und deiner Arbeitsgruppe treu geblieben bin, hast aber du selbst zu verantworten.
Es ist eine Freude, mit dir zusammenzuarbeiten. Danke!

Danke, Iwan. Du bist der beste Mentor, den man sich wünschen kann. Danke für all deine Zeit, deinen Ideenreichtum, deinen Einsatz und deine Engelsgeduld. Danke, dass du dich jeder Aufgabe mit vollem Elan und ganzem Herzen stellst und bei dir trotzdem niemand auf der Strecke bleibt.

Für die herzliche Aufnahme im Team und die geduldigen Erklärungen möchte ich euch allen aus der Arbeitsgruppe danken. Ganz besonders möchte ich dir, Sibel, Danke sagen. Du hast unermüdlich all meine Fragen beantwortet und warst immer für mich da, das schätze ich sehr. Ein besonderer Dank gilt auch Claudia und Nidhi, danke für das Suchen von Lösungswegen in komplizierten Situationen. Danke an Andi, Silke und Susann, für das Teilen eures reichen Wissens und des Laboralltags mit mir. Danke Melanie, danke Tobi, Mehari, Lisa und allen Studenten für die gute Zusammenarbeit und die angenehme Atmosphäre.

Danke, liebe Andrea. Deine Hilfsbereitschaft und dein Einsatz ist so unfassbar wertvoll und alles andere als selbstverständlich. Danke, dass du immer den Überblick behältst und du auch in den arbeitsreichsten Zeiten immer Zeit für ein gutes Wort findest.

Danke auch an alle Mitarbeiter des Instituts für Mikrobiologie und Hygiene, ganz besonders Gisela. Vielen Dank auch an Dirk Krause für die Koordination und an das DZIF für die Finanzierung.

Danke an meine Familie und meine Freunde für die bedingungslose Unterstützung. Insbesondere an meine Eltern, Großeltern, Renate und Hubert und an Sophie. Danke, dass ich immer willkommen bin.